nature communications

Article

https://doi.org/10.1038/s41467-026-69183-9

GID/CTLH E3 ligase complex control cell fate programs for sexual development of *Plasmodium falciparum*

Received: 16 October 2025

Accepted: 27 January 2026

Published online: 15 April 2026

Check for updates

Danushka S. Marapana[1,2,3] ✉, Sash Lopaticki[1,2], Balu Balan[1,2], Kitsanapong Reaksudsan[1,2], Simon A. Cobbold[1,2], Niall D. Geoghegan[1,2], Sachin Khurana[1,2], Stephen W. Scally[1,2], Peter Hickey[1,2], Niva Jayakrishnan[1,2], Vineet Vaibhav[1,2], Sukhdeep Spall[1,2], Jumana M. Yousef[1,2], Laura F. Dagley[1,2], Christopher D. Goodman[2], Anton Cozijnsen[2], Geoffrey I. McFadden[2], Kelly L. Rogers[1,2], Aaron Jex[1,2], David Komander[1,2], James S. McCarthy[1,2], Christopher J. Tonkin[1,2], Matthew W. A. Dixon[1,2,3] ✉ & Alan F. Cowman[1,2,3] ✉

Transmission of the malaria parasite *Plasmodium falciparum* requires the formation of specialised sexual cells called gametocytes. A hallmark of *P. falciparum* gametocyte development is its long duration, during which the parasite undergoes dramatic cellular remodelling including morphological, physiological and metabolic changes which result in the formation of a transmission ready, stage V gametocyte. Here we show that the PfGID E3 ubiquitin ligase complex regulates critical gametocyte cell fate programmes through the targeted ubiquitination of key proteins. Deletion of PfGID complex components leads to an arrest in gametocyte development and a loss of transmission to mosquitoes. PfGID governs gametocyte development by fine-tuning the protein levels of two substrates: the ZFP36 family RNAbinding protein GD1, and PfDPL, a cryptochrome-like protein. Our findings reveal that PfDPL regulates the expression of male-specific proteins early in gametocyte development that are essential for gametogenesis. In parallel to the PfDPL controlled cell fate program the RNA binding protein GD1 regulates transcripts crucial for gametocyte development by holding them in a state of translational repression. These findings illuminate the intricate molecular choreography underlying *Plasmodium* sexual development and provide insights into how single-celled eukaryotes execute cell-fate programmes to navigate complex life cycles and adapt to diverse host environments.

Plasmodium falciparum, the causative agent of the most severe form of malaria in humans, remains a significant global health challenge, with an estimated 282 million cases and 610,000 deaths reported in 2024[1]. Transmission of malaria requires the formation of specialised cells called gametocytes. Commitment to gametocytogenesis in *Plasmodium* species is governed by the epigenetic regulation of the transcription factor AP2-G[1,2]. Post commitment, *P. falciparum* gametocytes develop through 5 distinct morphological stages over approximately

[1]The Walter and Eliza Hall Institute of Medical Research, Parkville, Australia. [2]University of Melbourne, Melbourne, Australia. [3]These authors jointly supervised this work: Danushka S. Marapana, Matthew W. A. Dixon, Alan F. Cowman. ✉e-mail: marapana@wehi.edu.au; matthew.dixon@unimelb.edu.au; cowman@wehi.edu.au

10-12 days, resulting in the formation of mature male and female gametocytes which are capable of human to mosquito transmission. During the long development of *P. falciparum* gametocytes, the parasite not only undergoes dramatic morphological rearrangements characteristic of this species but also undergo dramatic remodelling of the parasite's physiology, metabolism and host RBC environment[3]. The timed orchestration of these biological programmes allows for the staged development of *P. falciparum* gametocytes, with disruption of any of these programmes resulting in arrested development and an inability to transmit to mosquitoes. Despite extensive knowledge of the key regulators of gametocyte commitment[4], little is known about the molecular mechanisms controlling the transcriptional and translational landscape driving *P. falciparum* gametocyte development.

Plasmodium falciparum has an expanded repertoire of RNA-binding proteins (RBPs) with ~13% of the genome encoding RBPs, compared to only 7.5% in humans[5]. Previous studies have shown an enrichment of RBPs during *Plasmodium* sexual development, with expression of 81 RBP genes being identified by in silico studies[6]. RBPs can regulate the translation of mRNA into protein through a process called translational repression, through the holding and timed release of transcripts for translation or by targeting transcripts for degradation[7]. The DEAD-box DDX6 RNA helicase DOZI (development of zygote inhibited) is the best characterised translational repressor in *Plasmodium* species, with functions in female gametocytes and the gamete to zygote transition[8]. In addition to DOZI, several other canonical RBPs, including CITH (CAR-I and trailer hitch homologue)[9], PUF1, PUF2 (pumilio-FBF family proteins)[10,11], and members of the ALBA (acetylation lowers binding affinity)[12] protein family, have also been shown to perform translational repression functions related to female gametocytes. In contrast, male gametocyte development depends on mRNA-stabilising deadenylase proteins such as CAF1 (CCR4-associated factor 1) and CCR4-1 1 (carbon catabolite repression 4-1), which are crucial in regulating mRNA stability and translation[13,14]. Recent studies in *Plasmodium berghei* have revealed multiple sex-linked proteins bearing zinc finger and Pumilio motifs, features characteristic of RNA-binding proteins involved in regulating translational repression[15].

The role of protein degradation through the ubiquitin-proteasome system, particularly via E3 ubiquitin ligase complexes[16], is a critical regulatory mechanism that has received little attention in *Plasmodium* biology. We hypothesised that ubiquitin-mediated protein degradation might orchestrate gametocyte development, through the targeted ubiquitination of key protein substrates, which facilitates the fine-tuning of key biological programmes. We focused on the glucose-induced degradation deficient (GID)/ C-terminal to LisH (CTLH) E3 ubiquitin ligase complex, which was discovered as a regulator of the transition of the closely related parasite *Toxoplasma gondii* from its acute tachyzoite form into the latent encysted bradyzoites[17].

The GID/CTLH complex plays a central role in protein homeostasis and cellular differentiation across eukaryotes[18,19]. In *S. cerevisiae*, its primary function is the signal-dependent ubiquitination of gluconeogenic enzymes, facilitating their degradation when glucose becomes available[18]. The complex is characterised by a RING (really interesting new gene) heterodimer and a modular assembly structure. In *S. cerevisiae*, three core proteins, GID1, GID5, and GID8, form a scaffold that supports the assembly of additional components. The RING heterodimer consists of GID2 and GID9, working in concert with an interchangeable substrate receptor (GID4, GID10, or GID11)[20]. GID7, once recruited to this assembly, promotes the formation of oligomeric complexes[21,22]. MOH1, also part of the GID complex in *S. cerevisiae*, has a human orthologue called YPEL5, which modulates the activity of the human CTLH complex[23–25].

Here, we characterise the *P. falciparum* GID complex (PfGID), showing that it is essential for gametocyte development and thus transmission. Our findings reveal that the PfGID complex is responsible for the ubiquitination of key proteins involved in gametocyte development, notably gametocyte development 1 (GD1) and deoxyribopyrimidine photo-lyase (PfDPL). We show that deletion of the cryptochrome-like protein PfDPL leads to the dysregulation of male-specific proteins required for fertilisation, while the RBP GD1 controls a separate cell fate programme through a translational repression mechanism. We show that the fine-tuning of PfDPL and GD1 through PfGID mediated ubiquitination regulates cell fate programmes underpinning *P. falciparum* gametocyte development and transmission.

Results

PfGID complex in *P. falciparum*

The *P. falciparum* GID complex components were identified using BLAST searches of the orthologous *Toxoplasma* GID/CTLH sequences against the *P. falciparum* genome. These searches identified six components PfGID1 (PF3D7_1014300), PfGID2 (PF3D7_0728600), PfGID7 (PF3D7_0518600), PfGID8 (PF3D7_1336400), PfGID9 (PF3D7_1330500), and YPEL5 (PF3D7_0925600), each showing a high degree of similarity to those found in yeast, *Drosophila* and humans (Supplementary Fig. 1a). Domain profiling of identified proteins revealed canonical domains typical of the GID/CTLH complex. PfGID1 contained a SPRY domain, PfGID7 contained a C-terminal WD40 domain and canonical RING domains were found within PfGID2 and PfGID9. PfGID8 along with PfGID9, featured CTLH domains found in GID/CTLH complexes. The identified PfYPEL5 protein showed similarity to other YPEL5 proteins and the *Drosophila melanogaster* Yippee protein[26], belonging to a conserved family of putative zinc-binding proteins.

To study these newly discovered GID/CTLH components in *P. falciparum* we generated cell lines in which the endogenous copy of the PfGID1, 7 and 8 components were tagged with a 3xHA tag or Flag-StrepII (in the case of PfGID8) at the C-terminus (Supplementary Fig. 1b–d). To facilitate investigation of the PfGID complex across both asexual and sexual blood stages, we made use of the inducible Gametocyte Producer 2 (iGP2) strain of *P. falciparum*, which utilises the conditional overexpression of the gametocyte development protein 1 (GDV1), for production of higher and more synchronous gametocytes compared to its parent strain NF54[27]. The expression and localisation of each HA- tagged PfGID component was confirmed by immunofluorescence assays performed on asexual blood-stage parasites and throughout gametocyte development (stage II, day 3; stage III, day 6; stage IV, day 9; and stage V 12-day). These experiments revealed a punctate cytoplasmic distribution of these proteins in asexual parasites and in gametocytes across all stages of development (stages I to V), with accumulation around and on the nucleus in late-stage gametocytes (Fig. 1a and Supplementary Fig. 1).

GID7 is a component of the core eukaryotic GID complex and proposed to regulate complex structure and stability. Therefore, we performed an anti-HA immunoprecipitation of PfGID7HA parasite lysate to confirm the identity of the GID complex in *P. falciparum*. LC-MS/MS analysis revealed PfGID7 interacted with PfGID1, PfGID2, PfGID8, PfGID9, and YPEL5 (Fig. 1b and Supplementary Data 1a, b). The components of the *P. falciparum* GID complex (PfGID) were validated using reciprocal immunoprecipitation of PfGID8-Flag-StrepII, which consistently identified the same complex components confirming the presence of a conserved GID/CTLH complex in *P. falciparum* (Supplementary Data 1c). The identification of PfGID1, 2, 7, 8, 9, and PfYPEL5 confirmed the presence of a core PfGID complex, orthologous to that identified in *Toxoplasma*[17].

PfGID is essential for transmission to mosquitoes

To elucidate the function of PfGID in *P. falciparum* development, we generated stable knockout lines for each of the genes encoding *Pfgid1, 2, 7, 8, 9* and *ypel5* (Supplementary Fig. 2a). Deletion of the *Pfgid*

https://doi.org/10.1038/s41467-026-69183-9

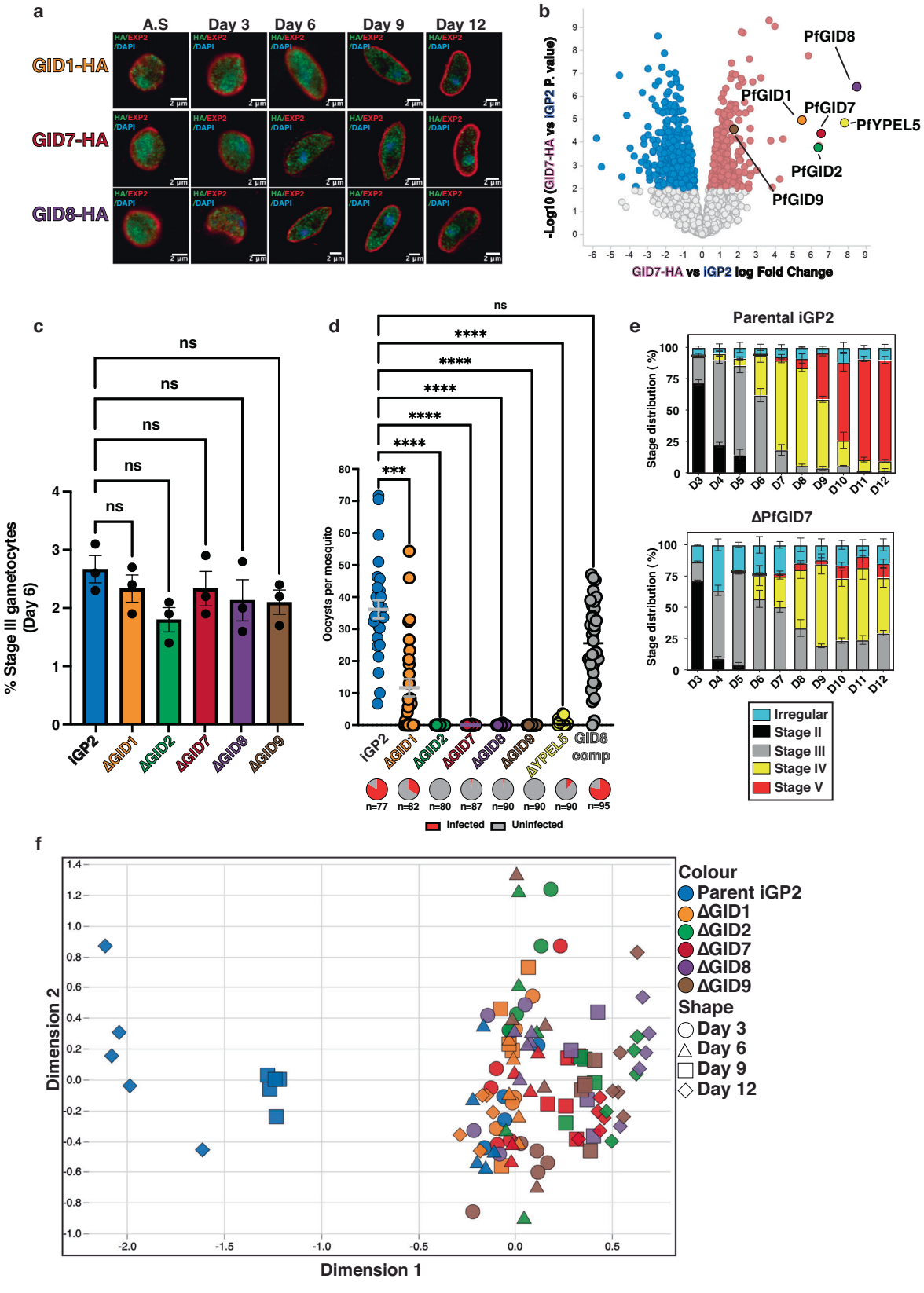

complex components had no impact on the growth of asexual blood-stage parasites, indicating that the complex was not essential for this part of the life cycle (Supplementary Fig. 2b and Supplementary Data 2a). To further confirm this lack of asexual growth phenotypes, we performed a 5-cycle competition assay (Supplementary Fig. 2c, Supplementary Data 2b). In this assay ΔPfGID7 parasites were mixed with an iGP2 parasite constitutively expressing mNeonGreen, and the composition of the parasite population monitored by flow cytometry. These experiments show no defect in the growth of the ΔPfGID7 parasite line compared to the parental line.

Next, we investigated if the *Pfgid* gene knockouts could produce gametocytes capable of transmission via mosquitoes. Deletion of each

Fig. 1 | Identification of a PfGID complex essential for gametocyte development in *P. falciparum*. **a** Immunofluorescence analysis of PfGID1-HA, PfGID7-HA, and PfGID8-HA parasite strains at asexual stages (A.S) and days 3, 6, 9, and 12 of gametocyte development. Tagged PfGID proteins (green), parasitophorous vacuole membrane (red), and DNA (blue) were visualised using α-HA, α-PfEXP2 antibodies, and DAPI staining, respectively. Scale bar = 2 μm. **b** Volcano plot of LC-MS/MS analysis comparing iGP2 and PfGID7-HA schizont stage parasite lysates after α-HA immunoprecipitation. Proteins with a significance cutoff of P-value ≤ 0.05 are shown, with those enriched in iGP2 or PfGID7-HA pulldown labelled with blue and pink circles, respectively. PfGID complex components are annotated with protein names. Data is from $n = 5$ biological replicates. **c** Day 6 (stage III) gametocyte production comparing iGP2 and ΔPfGID parasites shows no difference in differentiation and growth. Data are mean ± s.e.m. from $n = 3$ independent experiments and compared by ordinary one-way ANOVA (Kruskal-Wallis test). **d** Mosquito infection prevalence and oocyst intensity following day 12 gametocyte feed of iGP2, ΔPfGID1, ΔPfGID2, ΔPfGID7, ΔPfGID8, ΔPfGID9, ΔPfYPEL5, and PfGID8 complemented parasites. Data are mean ± s.e.m. from $n = 3$ independent experiments and compared by ordinary one-way ANOVA (Kruskal-Wallis test) with adjustment for multiple comparisons. $^{****}P < 0.0001$, $^{***}P = 0.0002$, n.s = not significant. **e** Stage distribution of iGP2 and ΔPfGID7 parasites across days 3-12 of gametocyte development (stage II to V). Data are mean ± s.e.m. from $n = 3$ independent experiments. **f** MDS plot of whole cell transcriptomes of day 3, 6, 9, and 12 gametocytes from iGP2, ΔPfGID1, ΔPfGID2, ΔPfGID7, ΔPfGID8, and ΔPfGID9 parasites. Data are from $n = 5$ biological replicates.

Pfgid component had no effect on commitment to gametocytes as no significant difference in the number of stage III gametocytes was observed between ΔGID and parent lines (Fig. 1c and Supplementary Data 2c). We next tested if the ΔPfGID1, 2, 7, 8, 9 and YPEL5 parasite lines, grown for the full 12 days of gametocytogenesis, were capable of transmission to mosquitoes, by assessing the number of oocysts in the knockouts compared to iGP2 control parasites. PfGID-deficient parasites, when fed to mosquitoes, were largely unable to generate the oocyst stage, with ΔPfGID2, ΔPfGID7, ΔPfGID8, and ΔPfGID9 producing no oocysts and ΔPfGID1 (12 oocysts/mosquito) and

YPEL5 (2 oocysts/mosquito) knockout parasites producing fewer oocysts than the parental line (Fig. 1d and Supplementary Data 2d). Complementation of the ΔPfGID8 parasites by reintroduction of a functional *pfgid8* gene restored transmission to mosquitoes, with no significant difference when compared to iGP2 parental line (Fig. 1d and Supplementary Fig. 2d, e).

PfGID is required for differentiation beyond stage III gametocytes

To define the precise stage of developmental arrest, we analysed ΔPfGID7 parasites, as GID7 acts as a core scaffold subunit whose loss destabilises the entire GID complex in other eukaryotes, providing the most conclusive readout of complex function during gametocytogenesis. Parental iGP2 and ΔPfGID7 parasites were induced to form gametocytes, and the stage distribution assessed daily throughout development (Fig. 1e and Supplementary Data 2e). While parental parasites developed normally, producing predominantly stage V gametocytes by day 12, ΔPfGID7 parasites exhibited a developmental arrest at the stage III-IV transition on day 6-7. A similar accumulation of stage III and IV gametocytes was observed for ΔPfGID1, 2, 8 and 9 parasite lines (Supplementary Fig. 2f and Supplementary Data 2f).

We next investigated this developmental block at the transcriptional level. We performed minibulk RNA-seq on iGP2 parental and all ΔPfGID parasite lines (ΔPfGID1, 2, 7, 8 & 9) at days 3, 6, 9, and 12 of gametocyte development, corresponding to stages II, III, IV, and V, respectively. Multi-dimensional scaling (MDS) analysis of the RNA seq data revealed a clear temporal trajectory in the parental line, with days 3 and 6 clustering closely before diverging sharply at days 9 and 12, reflecting the transcriptional reprogramming required for gametocyte maturation (Fig. 1f and Supplementary Data 3a–t). In striking contrast, all the ΔPfGID mutants (ΔPfGID1, ΔPfGID2, ΔPfGID7, ΔPfGID8, and ΔPfGID9), clustered with the early-stage groups days 3 and 6 but, critically, their day 9 and 12 profiles co-clustered with the day 6 timepoints (Fig. 1f and Supplementary Fig. 2g–j). These data support our morphological observations and confirm that the PfGID complex is essential for gametocyte development past stage III of development and their inability to transmit to mosquitoes.

PfGID function is required for male and female gametocyte differentiation

Previous work has identified a developmental branchpoint at around day 6 of development, which leads to the differentiation into male and female gametocytes. To evaluate the role of PfGID in male and female gamete development, we first analysed male gametogenesis, a process known as exflagellation. In the absence of PfGID2, 7, 8 and 9 there was a complete loss of exflagellation, while ΔPfGID1 parasites had reduced exflagellation rates compared to iGP2 (Supplementary Fig. 3a and Supplementary Data 2g). This showed that PfGID regulates developmental programmes required for the development of male gametes.

Sex-specific markers were used to further quantify gametocyte differentiation. To clearly distinguish male gametocytes, we generated a *P. falciparum* line expressing GFP under the control of the male-specific *mget* promoter and deleted *pfgid* genes within this background line (Supplementary Fig. 3b, c). The *mget* gene (PF3D7_1469900), which is highly transcribed in male gametocytes, served as a marker for male stage development[28]. Female gametocyte development was assessed by quantifying the expression of the female-specific protein Pfg377 (PF3D7_1250100) using immunofluorescence with specific antibodies (Supplementary Fig. 3d)[29,30].

We analysed the percentage of parasites exhibiting high MGET-GFP fluorescence intensity at day 12 (stage V male gametocytes) (Supplementary Fig. 3e and Supplementary Data 2h). The MGET transgenics, expressing either the normal PfGID complex or the complemented ΔPfGID8 parasites, showed approximately 27% and 30% high-intensity fluorescence, respectively, consistent with normal stage V male gametocyte development (Supplementary Fig. 3e, f). In contrast, ΔPfGID parasite lines (ΔPfGID1, 2, 7, 8, and 9) exhibited a significant decrease in gametocytes expressing high levels of MGET-GFP. The ΔPfGID1 line showed a partial phenotype with approximately 18% of parasites displaying high GFP fluorescence, while ΔPfGID2, 7, 8, and 9 lines showed < 2% (Supplementary Fig. 3e, f).

For female gametocyte differentiation, we quantified Pfg377 fluorescence intensity in the ΔPfGID parasites (Supplementary Fig. 3g). All ΔPfGID parasites showed significantly lower normalised Pfg377 intensity compared to the parental parasites. To assess overall gametocyte maturity, we quantified the expression of PfGAP45 (PF3D7_1222700), a sex-agnostic marker of the inner membrane complex (IMC)[31] in gametocytes (Supplementary Fig. 3h)[28,32]. All ΔPfGID parasites significantly reduced GAP45 intensity, indicating defective gametocyte development. Together, these results demonstrate that the PfGID complex was essential for the differentiation of both male and female gametocytes from stage III to stage V, underscoring its crucial role in *P. falciparum* sexual development.

ΔPfGID gametocytes show aberrant levels of proteins involved in mRNA processing, translation, and sex specification pathways

To further elucidate the phenotypic consequences of PfGID dysfunction, we conducted a global proteomic analysis comparing protein expression in ΔPfGID and iGP2 gametocytes at day 6 and day 12 of development. We initially evaluated the stability of the PfGID complex by quantifying protein abundance following targeted deletion of individual components. Notably, deletion of PfGID1, 7 or 8 led to a reduction in levels of all PfGID complex components, indicating their importance in maintaining the core scaffold integrity (Supplementary

Fig. 4a–c and Supplementary Data 4a–c). In contrast, deletion of the RING-domain containing subunits PfGID2 or 9 only affected their respective catalytic partners (Supplementary Fig. 4a–c), consistent with observations in mammalian GID/CTLH complexes[20,24,33]. Based on these findings, the ΔPfGID7 parasite line was mainly used for subsequent analyses.

To elucidate the broader impact of PfGID complex disruption on gametocyte development, we investigated the consequences of PfGID7 knockout on the proteome of day 6, stage III gametocytes, a pivotal timepoint identified in our phenotypic analyses (Fig. 1e)[34]. Quantitative proteomics detected 4110 proteins, of which 1541 were significantly up-regulated and 1092 significantly down-regulated. An unbiased gene ontology (GO) enrichment analysis was performed and showed a pronounced downregulation of proteins linked to core cellular processes, including mRNA processing, cytoplasmic translation and DNA replication, with an upregulation seen in proteins linked to nucleocytoplasmic transport and ribosome biogenesis. (Fig. 2a and Supplementary Data 4a, d). STRING cluster analysis of the same ΔPfGID7 proteome identified perturbations of ribonucleoprotein complexes assembly, spliceosomal factors, the translational machinery (ribosomal subunits and initiation factors), nuclear transport components (nucleoporins and importins), proteasome subunits (both core and regulatory particles) and cytoskeletal elements (dynein and microtubule-associated proteins) (Fig. 2b and Supplementary Data 4a, d). These findings suggest that mRNA processing, translation initiation, proteasome assembly, and RNP complex dynamics are essential for gametocytes to progress beyond stage III. This interpretation is supported by evidence from *Drosophila* and *C. elegans*, where disruption of the GID complex reduces ubiquitination of key translational repressors, leading to a collapse of developmental transitions and impaired cellular maturation[35,36]. This suggests an evolutionarily conserved mechanism whereby GID/CTLH complexes drive eukaryotic developmental transitions by regulating proteins involved in mRNA processing, translation initiation, and proteasomal degradation.

Previous work has shown that male and female gametocyte lineages are derived from a common sex less gametocyte progenitor. To further investigate if PfGID disruption is linked to male and female gametocyte development, we mapped previously identified male and female gametocyte-enriched proteins[28] onto our ΔPfGID7 proteome data (Fig. 2c and Supplementary Data 4a, e). ΔPfGID7 gametocytes show a strong, sex-specific proteomic shift: 283/446 male enriched proteins (~63%) are significantly down-regulated (Fisher's $p \approx 3.7 \times 10^{-68}$), compared with 166/469 female-enriched proteins (~35%) also down-regulated but with a more modest enrichment (Fisher's $p \approx 8 \times 10^{-6}$). In contrast, although 158/469 female proteins are up regulated, this enrichment was not statistically significant (Fisher's $p \approx 0.08$), showing that female factors do not disproportionately gain in abundance (Fig. 2c and Supplementary Data 4a, e). These results align with our phenotypic data showing that deletion of PfGID complexes affects both male and female gametocyte development programmes. This data suggests that the PfGID complex may function by directly regulating proteins to maintain mRNA turnover, translation and proteasomal clearance, which are required for both male and female gametocytes to form and to facilitate progression beyond stage III of development.

The PfGID complex is required for ubiquitination of GD1 and PfDPL

To identify potential ubiquitinated protein substrates of PfGID, we performed concurrent ubiquitinome and whole cell proteome analysis on day 12 gametocytes from iGP2, ΔPfGID1, 2, and 7 parasite lines (Supplementary Data 4f, g). We observed decreased ubiquitination and protein levels of PfGID1, 2, and 7 in a PfGID-dependent manner (Supplementary Fig. 4d–f). While this pattern is compatible with PfGID acting as an E3 ubiquitin ligase capable of autoregulation via self-ubiquitination, a feature observed in other systems[37], it may also reflect decreased stability of the remaining complex following subunit loss.

To identify high confidence, PfGID substrates, we selected candidates that showed an increase protein abundance but had a significant decrease in both the number and abundance of ubiquitinated peptides in the ΔPfGID1, 2 and 7 parasite lines compared to iGP2 controls (Supplementary Data 4f, g). In addition, we further focused on substrates that were identified in all three knockouts and had multiple ubiquitinated peptides. Using these stringent criteria, two potential PfGID substrates were identified: deoxyribopyrimidine photo-lyase (PfDPL) (PF3D7_0513600) and gametocyte development 1 (PfGD1, subsequently referred to as GD1 to prevent confusion with components of PfGID (PF3D7_0927200)[15] (Fig. 2d, Supplementary Fig. 4g, h and Supplementary Data 4f, g). In the absence of ΔPfGID7 function, we observed 1.5- and 1.7-fold increases in PfDPL and GD1 protein levels, respectively. Consistent with both these proteins being PfGID-dependent substrates, we identified eight ubiquitinated peptides in PfDPL and three ubiquitinated peptides in GD1 that decreased between 2- and 8-fold within the ΔPfGID7 parasite line (Fig. 2d).

PfDPL exhibits structural characteristics of both photolyase and cryptochrome proteins, featuring canonical PL/CRY and FAD domains, along with a C-terminal extension typical of cryptochromes[38] (Fig. 2e). GD1 was previously identified as being essential for gametocyte development in *P. berghei*[15]. GD1 has a CCCH zinc finger protein domain found in ZFP36 RNA-binding protein (RBP) family members (Fig. 2 f)[15]. Ubiquitinated peptides for both PfDPL and GD1 mapped to the intrinsically disordered regions within the proteins away from the annotated functional domains (Fig. 2e, f, Supplementary Fig. 5a, 6a and Supplementary Data 4f, g). Importantly, mRNA transcription levels of both PfDPL and GD1 showed no significant differences between iGP2 and ΔPfGID parasites during gametocytogenesis (Fig. 2g), suggesting post-translational regulation of these substrates.

To determine the importance of PfDPL and GD1 in gametocyte development, we generated ΔPfDPL and ΔGD1 parasite lines (Supplementary Fig. 4i, j). While both lines were able to develop in asexual stages, both exhibited significant defects in transmission to mosquitoes (ΔPfDPL, 8 oocysts/87 mosquitoes; ΔGD1, 1 oocyst/92 mosquitoes) (Fig. 2h and Supplementary Data 2d). These results indicate that both PfDPL and GD1 are essential for the transmission of sexual stages between the human and mosquito hosts and consistent with the phenotypes observed following disruption of the PfGID complex.

The PfGID complex regulates PfDPL levels and expression of male gametocyte transmission factors

To investigate the protein expression pattern and localisation of PfDPL throughout the parasite life cycle, we created a PfDPL-HA tagged line. Immunoblotting analysis of PfDPL-HA parasites identified protein expression in asexual blood stage parasites and gametocytes, with peak expression at day 4 (stage II) of gametocyte development (Supplementary Fig. 5c). Immunofluorescence studies showed PfDPL localised close to the nucleus in asexual stage parasites but nuclear and cytoplasmic in sexual stages (Fig. 3a and Supplementary Fig. 5d). PfDPL contains putative bi-partite nuclear localisation sequences as observed in mouse, human and *Arabidopsis* cryptochrome proteins (Supplementary Fig. 5b)[39–41]. Consistent with this, at day 4 of gametocyte development, PfDPL was observed in the nucleus and alongside the nascent microtubular network (Fig. 3a and Supplementary Fig. 5d).

To understand the function of PfDPL we performed co-immunoprecipitation experiments on samples collected from PfDPL-HA and iGP2 parental parasites at day 4 of gametocyte development. The samples were analysed by mass spectrometry and the protein significantly enriched in the PfDPL-HA samples interrogated by GO and pathway enrichment analysis (Fig. 3b and Supplementary Data 1d). This

https://doi.org/10.1038/s41467-026-69183-9

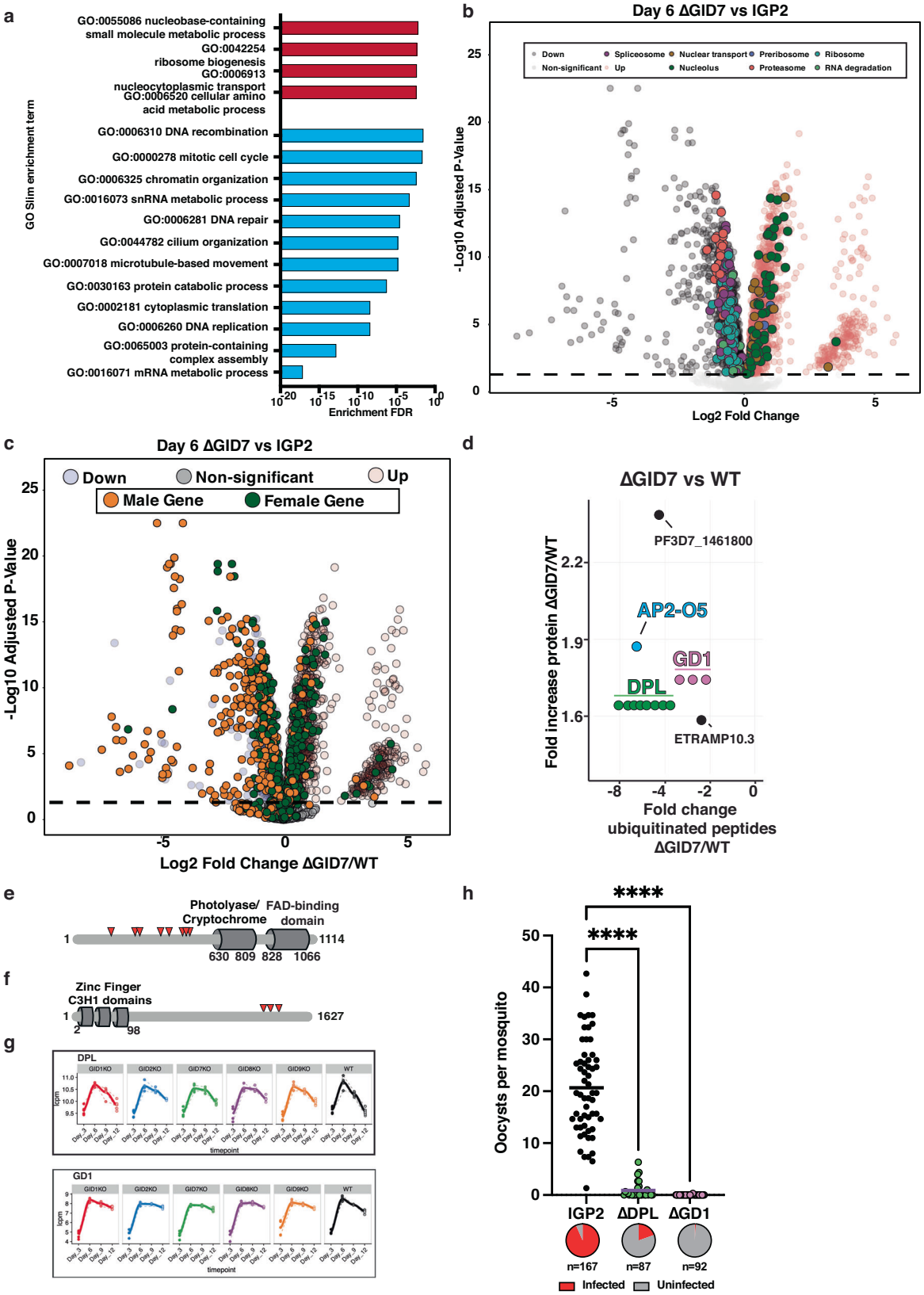

revealed a broad spectrum of PfDPL-associated factors: core components of the mRNA synthesis and co-transcriptional machinery (including RNA polymerase II subunits RPABC1 and RPABC2, spliceosomal proteins and RNA-metabolic enzymes), ribosome biogenesis and translation initiation factors, and multiple ubiquitin– proteasome proteins indicative of targeted proteostasis. In parallel, PfDPL pulled down proteins involved in vesicle-mediated transport, mitochondrial tricarboxylic acid (TCA)-cycle enzymes and oxidative-phosphorylation complexes, suggesting a link between PfDPL and the known physiological and metabolic changes known to occur during gametocyte maturation, however these interactions require further experimental validation.

Fig. 2 | ΔPfGID gametocytes show aberrations in proteins involved in mRNA processing, translation, and sex specification. a Gene Ontology Slim (GO) terms enrichment of day 6 ΔPfGID7 proteome showing highly significant (< 0.05 FDR) upregulated (red) and downregulated (blue) pathways. **b** Volcano plot of whole cell proteome in day 6 ΔPfGID7 vs iGP2 parasites, with proteins from most significantly altered STRING clusters mapped. **c** Volcano plot of whole parasite proteome in day 6 ΔPfGID7 vs iGP2 parasites, with key sex-specific proteins mapped. **d** Proteins isolated by anti-diGly antibody enrichment from day 12 ΔPfGID7 and parental iGP2 gametocytes. Proteins with at least a 50% increase and 2-fold decreased ubiquitinated peptides in ΔPfGID7 compared to parental cells are displayed. Individual proteins are annotated, and each circle corresponds to an individual ubiquitinated peptide. PfDPL and GD1 peptides are highlighted with green and purple circles, respectively. **e** Domain structure of PfDPL with photolyase/cryptochrome and FAD-binding domains. Ubiquitination sites are marked with red arrows. **f** Domain structure of GD1 with N-terminal CCCH Zinc finger domains and ubiquitination sites marked with red arrows. **g** mRNA transcription profile of PfDPL and GD1 across days 3, 6, 9, and 12 in iGP2 parental and ΔPfGID1-9 gametocytes as identified by RNAseq. Data is from $n = 5$ biological replicates. **h** Mosquito infection prevalence (within the box) and oocyst intensity following day 12 gametocyte feed of iGP2, ΔPfDPL, and ΔGD1 parasites. Data in (**b**, **c**) are from $n = 5$ independent experiments. Data in (**h**) are mean ± s.e.m. from $n = 3$ independent experiments and compared by ordinary one-way ANOVA (Kruskal-Wallis test).

Critically, PfDPL co-purified with a suite of chromatin remodelling proteins including core histones H2A, H2B and H4; a histone deacetylase; nucleosome assembly factors; FACT complex subunits SSRP1 and SPT16; and high-mobility group protein B2 – showing an association of DPL with modulators of chromatin, transcription and co-transcriptional processing[42]. The simultaneous association with nuclear-pore constituents (NUP313, NUP138, NUP637 & NUP176) and cytoskeletal elements (α-, β- & γ-tubulin) further implies that PfDPL may participate in nucleocytoplasmic trafficking and spatial organisation of the transcriptional apparatus (Fig. 3b and Supplementary Data 1d). Together, these data suggest a model in which PfDPL forms part of a multiprotein complex that integrates chromatin remodelling, mRNA processing, ubiquitin–proteasome–mediated proteostasis and energy metabolism, echoing functional paradigms described for eukaryotic cryptochromes[42].

To test if the presence of PfGID7 could modulate PfDPL expression, we introduced a ΔPfGID7 deletion into PfDPL-HA parasites. We demonstrated by immunoblot that throughout gametocyte development (days 2, 6, 8 and 12), PfDPL protein levels were consistently regulated by PfGID (Fig. 3c, d). We observed at least a 2-fold increase in PfDPL protein levels in the PfDPL-HA(ΔPfGID7) parasites compared to PfDPL-HA parental parasite controls at all time points tested. Interestingly, while both PfDPL and PfGID are expressed during asexual stages, we could not detect PfGID-dependent regulation of PfDPL at either the trophozoite or schizont stage of growth (Supplementary Fig. 5e, f).

To further understand the functional consequences of this PfGID-mediated regulation and the role of PfDPL in gametocyte development, we analysed the total cellular proteomes of iGP2 and ΔPfDPL parasites at both days 6 and 12 of development. A principal component analysis (PCA) of these proteomes shows close clustering of both cell lines at day 6 and separated populations at day 12 (Fig. 3e and Supplementary Data 4h, i). This pattern suggests the loss of PfDPL has a more pronounced effect on the proteome of late-stage gametocytes. This observation was consistent with the transmission defect observed in ΔPfDPL parasites (Fig. 2h).

To better understand this link and the pathways being affected following PfDPL deletion, GO enrichment analyses of both the day 6 and day 12 data was performed. This identified highly significant decreases in multiple pathways that govern male gametocyte development within the ΔPfDPL parasites (Fig. 3f, Supplementary Fig. 5g and Supplementary Data 4j, k). Specifically, proteins essential for DNA replication (ORC1), mitotic cell cycle (CRK5), DNA repair (RFC1), microtubule function (kinesin8-B) and cell division (EB1) were significantly decreased at both time points in the ΔPfDPL (Supplementary Fig. 5g). In addition, the GO term 'reproductive process' showed significant decreases at day 12 in ΔPfDPL gametocytes compared to parental controls (Fig. 3f). Consistent with this, we identified a significant PfDPL-dependent decrease in the protein levels at day 6 and 12 of PfHAP2 and PfHAP2p proteins which are essential for male gamete fusion during fertilisation (Supplementary Fig. 5g). Interrogation of the data, viewed through the lens of known male and female specific proteins[28], showed that half the down regulated proteins identified in the ΔPfDPL gametocytes were linked to male development

(224/446 or 50.5% of male-specific proteins) with very few female proteins being regulated (12/469 or 2.5% of female-specific proteins) (Fig. 3g). This suggests that PfDPL protein level is critical for regulating the expression of proteins required for male gametocyte development and gamete function. When analysing genes known to drive *P. falciparum* male or female lineage[43], ΔPfDPL gametocytes exhibit at least a 2-fold decrease in protein expression of 13/14 male driver genes, while only 2/14 female drivers showed a similar change (Fig. 3h).

The phenotypic appearance of these molecular signatures of male gametocyte developmental defects was then functionally investigated using male gametogenesis (exflagellation) assays (Fig. 3i and Supplementary Data 2g). ΔPfDPL parasites showed a drastic reduction in their capacity to undergo exflagellation compared to the parental control, reinforcing the critical role of PfDPL in male gametocyte development. The findings suggest that the putative cryptochrome PfDPL plays a crucial role in regulating gene expression and male cell fate during gametocyte development. The controlled regulation of PfDPL by PfGID throughout gametocytogenesis, but not in asexual stages, highlights the stage-specific nature of this regulatory mechanism and its importance in sexual stage development and transmission.

GD1 abundance modulates translational repression complex dynamics

We next interrogated the function of GD1, the second PfGID regulated protein identified by our ubiquitomics analysis. We endogenously tagged the C-terminus of GD1 with a 3xHA and mScarlet tag (GD1-HA-mScarlet) and investigated its expression and location by immunofluorescence assay (IFAs). GD1 could not be detected during the asexual blood stages of development, but was expressed across gametocyte development (days 3, 6, 9, & 12), localising into distinct puncta within the parasite cytoplasm (Fig. 4a and Supplementary Fig. 6b).

Next, we investigated if the ubiquitination of GD1 by the PfGID complex regulated protein levels across gametocyte development. To do this, we deleted PfGID7 in the GD1-HA-mScarlet parasite line and tracked GD1-HA-mScarlet protein expression across gametocyte development using flow cytometry in both parental and ΔPfGID7 parasite backgrounds (Fig. 4b). In parental control parasites, GD1-HA-mScarlet expression began at day 3, peaked at day

5, and then declined as gametocytes reached maturity at day 12. In ΔPfGID7 parasites, GD1HA-mScarlet expression followed a similar initial pattern in the early stage of gametocytogenesis but peaked a day later (day 6) and showed increased stability for the remainder of development, with at least a ~ 2-fold increase in expression compared to parental parasites. These results are consistent with GD1 playing a role in sexual development regulated by PfGID through ubiquitination of the C-terminal end of the protein.

https://doi.org/10.1038/s41467-026-69183-9

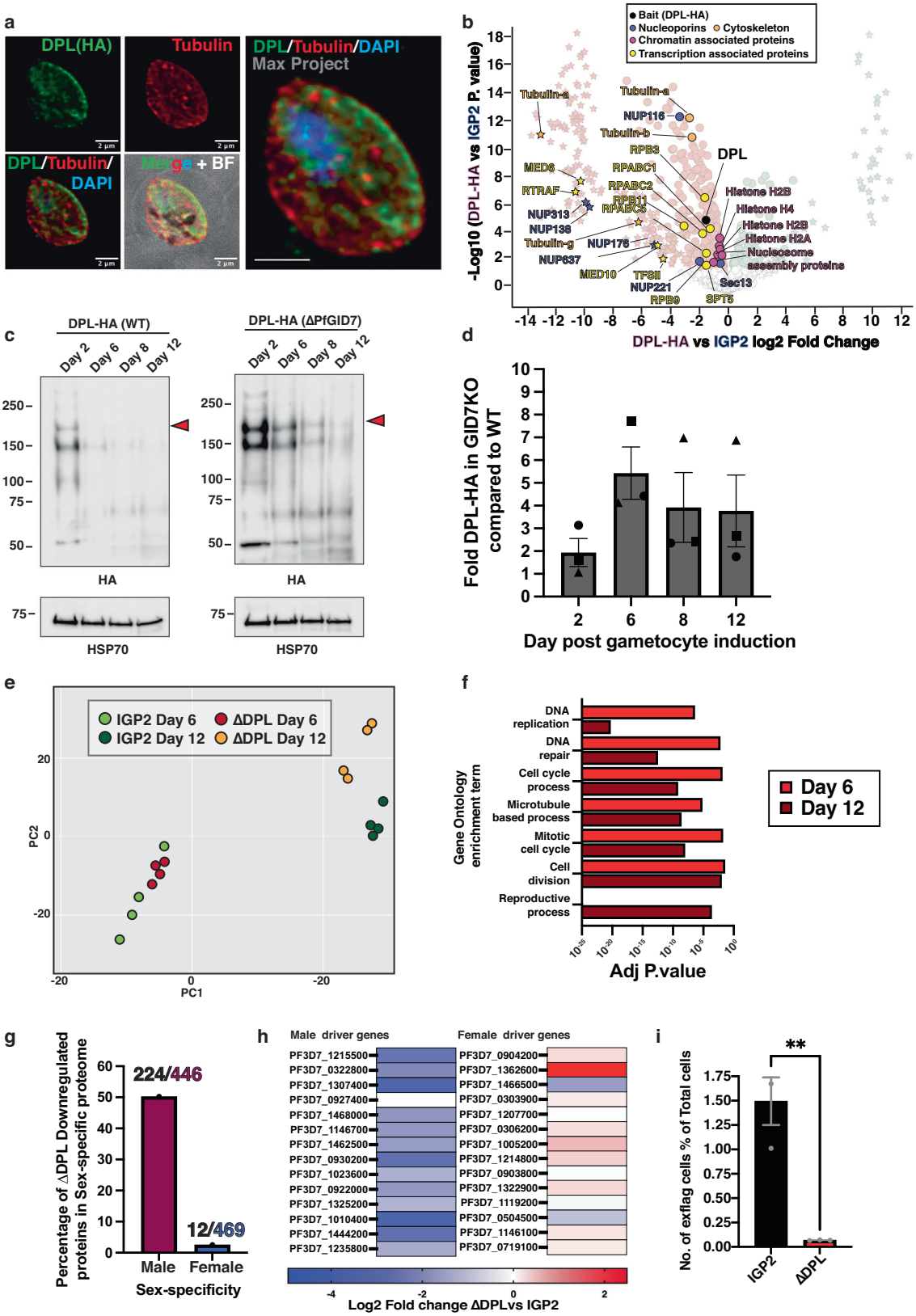

To further investigate GD1 function, we performed immunoprecipitation experiments on GD1HA-mScarlet gametocytes (and parental controls) collected at days 3, 6, and 9 of gametocyte development. Analysis of the immunoprecipitates by LC-MS/MS identified significantly enriched proteins and revealed a dynamic network of GD1 interactions, suggesting it may have a role in P-body formation, consistent with GD1 containing a zinc finger RNA-binding domain. (Fig. 4c and Supplementary Data 1e–g). P-bodies, or processing bodies, are cytoplasmic ribonucleoprotein (RNP) granules that control mRNA decay and translational repression[44]. At day 6 of gametocytogenesis, the GD1 interactome incorporates CAF40 and DCP1, suggesting the formation of a repressive P-body-like structure. CAF40 (CCR4-NOT

Fig. 3 | The cryptochrome protein DPL regulates the expression of male gametocyte cell fate. a Localisation of PfDPL-HA at Day 4 of gametocyte development. PfDPL, microtubules and DNA levels were visualised with α-HA, α-Tubulin and DAPI, respectively. **b** Volcano plot of LC-MS/MS analysis of iGP2 and PfDPL-HA strain day 4 gametocyte lysate by α-HA immunoprecipitation. Proteins with a significance cutoff of *P*-value ≤ 0.05 and enriched in iGP2 or PfDPL-HA pulldown labelled with green and red colours, respectively. Proteins only isolated in DPL-HA IP and iGP2 parasites labelled with red and green stars, respectively. *P. falciparum* proteins homologous to known functional interactors of cryptochromes are highlighted. **c** Western blot of PfDPL-HA expression gametocyte stage of PfDPL-HA (parental) and PfDPL-HA (*Δgid7*) strains. PfDPL was detected using α-HA antibodies, with α-HSP70 was used as a loading control. **d** Bar graph shows quantification of data with mean ± s.e.m. from $n = 3$ independent experiments. **e** Principal Component Analysis (PCA) plot of day 6 and day 12 ΔPfDPL and iGP2 parasites upon analysis of the total cellular proteome. Data are from $n = 4$ biological replicates. **f** Selected Gene Ontology (GO) terms showing highly significant male gametocyte development pathways of down regulated proteins at day 12 ΔPfDPL upon analysis of total cellular proteome. **g** Appearance of proteins decreased in levels for day 12 ΔPfDPL parasites within identified male and female specific proteins. **h** Heatmap of the expression of key male and female lineage driver genes at day 12 ΔPfDPL vs iGP2 parasites as identified by mass spectrometric analysis of total cellular proteome. **i** Analysis of the exflagellation rate of day 12 gametocytes of ΔPfDPL and iGP2 strain parasites. Data are mean ± s.e.m. from $n = 3$ independent experiments and compared by unpaired two-sided t-test analysis. $^{**}P = 0.0043$.

complex subunit 7) is a core component of the CCR4-NOT deadenylase complex, essential for mRNA decay and translational repression in P-bodies[45,46]. DCP1 (decapping enzyme 1) is a critical factor in mRNA decapping, another key process in P-body-mediated mRNA degradation[47]. The presence of these proteins in the GD1 complex strongly indicates the formation of functional P-bodies at this stage of gametocyte development. By day 9, the repressive capacity of the P-body diminished, which coincided with the concomitant PfGID-dependent degradation of GD1. This dynamic regulation of P-body components is consistent with observations in other eukaryotic systems, where P-body assembly and disassembly are tightly controlled processes that respond to cellular needs for mRNA storage or degradation[48].

To functionally test the role of GD1 in gametocyte development, we performed stage distribution assays as described above. ΔGD1 parasites underwent arrest in development as early as day 4, during the stage II-III transition (Fig. 4d, Supplementary Fig. 6c and Supplementary Data 2e). As the level of RNA binding protein is critical for functional P-body formation[44] we created an additional transgenic parasite line overexpressing GD1 (GD1-OE) under the control of the strong sexual stage-specific promoter Pfs16[49] (Supplementary Fig. 6d). We hypothesised that GD1 overexpression by means of a second protein copy, should phenocopy ΔPfGID7 parasites, whereby a lack of ubiquitination leads to increased GD1 abundance, and lead to disrupted P-body dynamics and gametocyte developmental arrest. To test this, we initiated gametocyte assays in the GD1-OE parasites and assessed the stage distribution across development (Fig. 4d). Analysis of the data shows a striking arrest of parasites at around day 5 of development, which is consistent with our previous results showing that ΔPfGID7 parasites with increased GD1 abundance arrest by day 7 of development (Figs. 1e, 4d and Supplementary Data 2e). These results demonstrate that either insufficient (ΔGD1) or excessive levels of GD1 (ΔPfGID7 and GD1-OE) impair gametocyte development, confirming that precise regulation of GD1 levels are essential for normal gametocyte progression. Interestingly, immunofluorescence microscopy revealed that increased levels of GD1 in either ΔPfGID7 or GD1-OE lines did not affect GD1's ability to form cytoplasmic puncta within gametocytes, suggesting that GD1 levels do not regulate P-body formation and instead may regulate P-body protein composition (Supplementary Fig. 6f).

To gain further insight into this mechanism, we performed proteomic analysis of ΔGD1 parasites (day 5), GD1-OE (day 5), and ΔPfGID7 (day 6), at which stage GD1 levels were 0.05, 2.45 and 1.65-fold compared to GD1 in parental controls (Supplementary Fig. 6f and Supplementary Data 4l, m). To gain further insight into this mechanism of GD1-mediated parasite arrest, we then investigated the homeostasis of P-body proteins within these variant cell lines. Surprisingly, we found that changes in GD1 levels, either by deletion or accumulation, resulted in the downregulation of translational repression proteins, including core repressive components DDX6, CAF40, and PUF1 (Fig. 4e). DDX6, along with its partner protein TRAIL (also known as DOZI and CITH respectively in *Plasmodium* species) is a key helicase involved in P-body formation and function[8,9,11,50].

These results identify GD1 plays a critical role in the dynamic assembly of a protein complex, enriched in components of P-bodies and translational repression, suggesting that GD1 is likely functioning in a P-body controlling translation of mRNAs vital for gametocyte development and transmission.

GD1 controls gametocyte cell fate through translational repression in gametocytes

Our analysis has shown that GD1 as a component of P-body complexes, interacting with the CCR4-NOT complex, DOZI (DDX6), LSM-14 (trailer hitch), PUF1, mRNA de-capping enzymes, and other classical P-body components (Fig. 4c). This is supported by data from *P. berghei* confirming these interactions[15]. To define the mRNA cargo associated with the GD1 P-body complex, we performed RNA immunoprecipitation sequencing (RIP-Seq) on GD1-HA pulldowns collected at day 5 of gametocyte development, a stage when GD1-mediated translational repression is expected to be active. The RIP-seq revealed 489 transcripts that were significantly enriched relative to the input control after Gaussian mixture modelling of enrichment ratios (LOD > 0) (Fig. 5a and Supplementary Data 3u). In these analyses, transcripts with LOD > 0 is considered significantly enriched with the RNA binding protein[51]. DBSCAN clustering of GD1-bound transcripts showed significant enrichment of functional classes related to RNA metabolism, protein metabolism, translational factors, and ribosomes (Supplementary Fig. 7a, b and Supplementary Data 3u). In addition, mRNAs of several proteins previously shown to be crucial for gametocyte development and transmission were enriched, including g27/25, md3, AP2-domain regulators, chromatin regulators, protein translation and mitochondrial energetics transcripts (Supplementary Fig. 7b and Supplementary Data 3u).

To identify GD1-associated transcripts undergoing translational repression, we searched transcriptomic and proteomic datasets from day 6 parental and ΔPfGID7 gametocytes. Among the 489 GD1-associated transcripts, 320 (~65%) were significantly differentially transcribed between day 6 and day 3 (Fig. 5b–d and Supplementary Fig. 7c). Notably, 16 of these showed no significant change at the transcript level between day 6 parent and ΔPfGID7 parasites but were upregulated at the protein level in ΔPfGID1, 2 and 7 parasites compared to parent, indicating a defect in translational repression and aberrant protein expression (Fig. 5b–f and Supplementary Fig. 7c–g).

Given that ΔPfGID7, ΔGD1 and GD1 overexpression parasites all displayed markedly reduced levels of DDX6 (Fig. 4e)—an RNA helicase implicated in the translational repression of gametocyte transcripts in *Plasmodium*[8] identified in our study as a robust GD1 interactor (Fig. 4c)—we systematically assessed the consequences of PfGID7 depletion on the expression of canonical DDX6-associated, translationally repressed transcripts. We found 475 transcripts from previously published DDX6 RIP-Seq data[52] upregulated within ΔPfGID7 parasites, including

https://doi.org/10.1038/s41467-026-69183-9

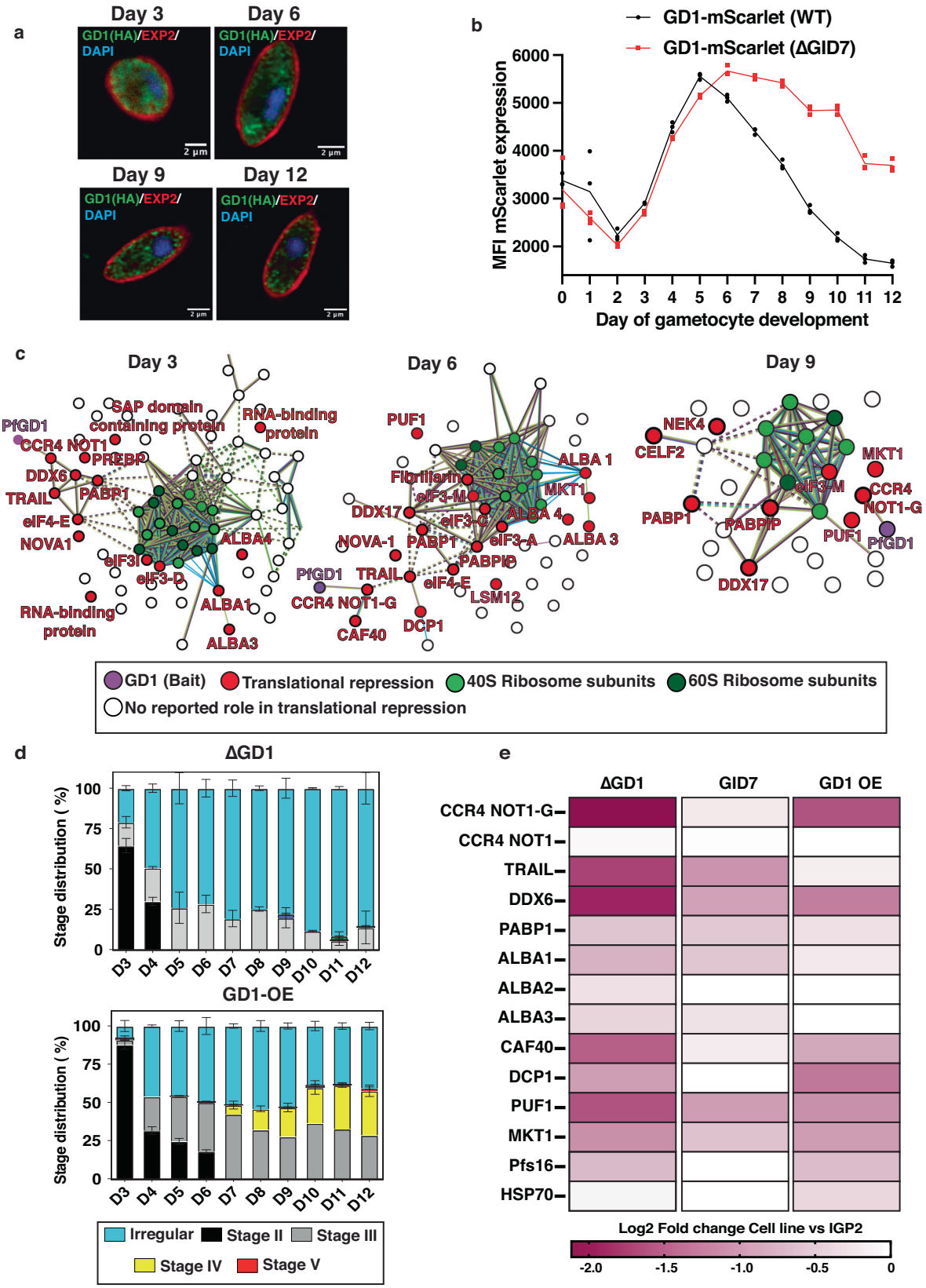

female development factors, AP2 transcription factors, and other cell fate regulators (Supplementary Fig. 7h). These findings indicate that GD1 exerts broad posttranscriptional control during gametocytogenesis by interacting with P-body components and mRNAs, consistent with P-body-driven regulatory mechanisms in model organisms[53]. Collectively, our data show that the PfGID complex maintains GD1 at a precise "Goldilocks" concentration via ubiquitination, controlling the repression and release of GD1-bound transcripts. The loss of PfGID complex (and targeted ubiquitination) disrupts GD1-mediated RNA repression, leading to premature release and expression of cell-fate transcripts, stalling gametocyte progression by misaligning key developmental events.

Fig. 4 | GD1 is an integral component of a dynamic translational repression complex. a Localisation of GD1-HA-mScarlet in days 3, 6, 9 and 12 of gametocytes. GD1, parasitophorous vacuole membrane (PVM) integrity, and DNA levels were visualised with α-HA, α-PfEXP2, and DAPI, respectively. **b** Mean Fluorescent Intensity of mScarlet expression during gametocyte development of GD1-HA-mScarlet in iGP2 parental and ΔPfGID7 parasites. **c** GD1-HA-mScarlet immunoprecipitation from day 3 (left), day 6 (middle), and day 9 (right) gametocytes. All significantly enriched proteins at each day are displayed in a network analysis map. *P. falciparum* proteins homologous to known eukaryotic translational repression components and ribosomal proteins are highlighted. **d** Stage distribution of ΔGD1 and GD1 increased expression (OE) parasites across days 3-12 of gametocyte development. **e** Heatmap of the expression of selected key translational repression proteins identified by GD1-HA immunoprecipitation as observed in Day 5 total proteomes of ΔPfGD1 and GD1-OE and day 6 of ΔPfGID7 parasites compared to iGP2 control cells. Data in c and e are mean ± s.e.m. from $n = 5$ independent experiments.

Discussion

P. falciparum relies on a precisely orchestrated life cycle to ensure transmission across its two hosts and therefore spread and multiplication. A critical juncture in this cycle is the development of the mature sexual stage gametocytes, which are the only stage capable of transmission from the human host to the mosquito host. Gametocyte development in *P. falciparum* is unique, with the parasite undergoing dramatic changes to its morphology, physiology and metabolome over ~12 days of development[4]. Despite significant progress, the regulatory mechanisms controlling the transcription and translation of key genes and proteins that drive these unique biological programmes remain poorly defined and represent a critical gap in our understanding. Our analyses were conducted in the GDV1-inducible iGP2 system[27], which enables synchronous gametocyte production but may not fully recapitulate natural commitment, and future studies will be needed to evaluate PfGID function in a wild-type setting.

Our study reveals that the PfGID complex, while not being essential for asexual stage growth and gametocyte commitment, regulates biological pathways during gametocyte development through the targeted ubiquitination of key substrate proteins. This adds to the growing evidence highlighting the importance of E3 ubiquitin ligases in controlling cell fate across eukaryotes. In addition, our analyses revealed PF3D7_1033900 as a strong candidate for the cognate E2 ligase of the PfGID complex. Its conservation with the UBE2H/UbcH2 family—well-established E2 ligases of GID/CTLH complexes in other eukaryotes—suggests that PfGID likely employs a similarly conserved ubiquitination mechanism. Our findings parallel observations in diverse organisms, including *Drosophila*, humans, yeast, and *T. gondii*[17], demonstrating the pivotal and evolutionarily conserved role of the GID complex in orchestrating cellular differentiation[22]. In the context of Apicomplexan parasites, this regulatory mechanism is crucial to coordinate the complex developmental transitions required as the parasites move from rapidly dividing (asexual stages and tachyzoites) to latent forms (gametocyte and bradyzoite) in the life cycle.

Our study has identified two key protein substrates, PfDPL and GD1 that control separate biological programmes essential for gametocyte development and transmission (Fig. 6). The posttranslational regulation of these substrates by the PfGID E3 ubiquitin ligase complex allows for rapid and precise control of protein levels during developmental transitions, such as those required during *P. falciparum* gametocyte development. PfDPL has homology to cryptochrome/photolyase DNA-binding proteins. Consistent with this, PfDPL has a nucleocytoplasmic localisation and interacts with chromatin-associated proteins suggest a complex regulatory mechanism (Fig. 6). Several of the key PfDPL protein interactors include the histone proteins, histone deacetylase, nucleosome assembly proteins, FACT complex components and co-transcriptional machinery. These proteins, along with PfDPL, are specific interactors with the chromatin remodelling protein PfSnf2L, which organises a just-in time transcriptional programme for stage-specific genes[54]. This conservation of the interactome allows us to propose PfDPL as a putative chromatin remodeller, initially organising male-specific genes into a common nuclear domain[55,56] (Fig. 6). As gametocytes mature and PfDPL levels decrease due to PfGID-mediated ubiquitination, this spatial clustering may prime these genes for coordinated activation (Fig. 6). This hypothesis aligns with emerging concepts in spatial genome organisation[57] and suggests a sophisticated mechanism for temporal and spatial control of gene expression during gametocytogenesis (Fig. 6).

In this work, we show that deletion of PfDPL leads to a reduction of proteins required for male gametocyte development and microgamete formation and function[11,28]. Surprisingly, it appears that this biological programme is being regulated early in gametocyte development. While the exact function of PfDPL remains to be elucidated, its similarity to cryptochromes suggests a potential role in response to environmental stimuli[58]. This is important in the context of gametocyte development, which must be precisely timed for successful transmission. Early-stage gametocytes circulate in the blood stream, while stage II-IV gametocytes are sequestered in the spleen and bone marrow, it is plausible that PfDPL may set the rhythm of cellular development early in development, allowing for the timed release of sex ready stage V gametocytes (Fig. 6). The regulation of PfDPL by PfGID could represent a mechanism for finetuning the parasite's responsiveness to environmental signals throughout its developmental cycle. Strikingly, the strong homology between PfGID7 and the *Drosophila* E3 ligase Ramshackle/BRWD3, which orchestrates cryptochrome ubiquitination to maintain circadian periodicity[59] points to an evolutionarily conserved role for GID-mediated proteostasis in temporal regulation. These findings strongly suggest that *P. falciparum* may deploy ubiquitin–proteasome–driven oscillatory programmes to coordinate key developmental transitions, including gametocytogenesis. Elucidating such regulatory networks could reveal an entirely new layer of temporal control in parasite biology and open avenues for chronotherapeutic intervention.

In contrast to PfDPL, the second substrate protein GD1 is an RNA-binding protein that locates to P-body structures and regulates translational repression processes, facilitating gametocyte development (Fig. 6). GD1 emerges as a central regulator of P-body dynamics, with both increased and decreased levels leading to alterations in key P-body components. This bidirectional sensitivity highlights the role of GD1 as a molecular rheostat, fine-tuning the composition and function of these mRNA regulatory hubs (Fig. 6). In addition to binding transcripts related to ribosomal subunits and mitochondrial function, GD1 also controls the expression of key cell fate transcripts, including *pfg25/27*[60] and *md3*[15], as evidenced by our RIP-seq analysis. The formation of GD1-mediated P-bodies correlates with the reduction of Pfg25/27 and MD3 proteins, suggesting that specific translational repression of these transcripts at day 6 permits gametocyte maturation. This day 6 checkpoint likely commits immature parasites towards sexual specification, with the PfGID-GD1 axis orchestrating a temporally coordinated programme of translational repression and mRNA storage (Fig. 6).

The presence of ubiquitination within the intrinsically disordered regions (IDRs) of both GD1 and PfDPL provides insight into the molecular mechanisms underlying their regulation by the PfGID complex. IDRs can serve as flexible platforms for protein-protein interactions and posttranslational modifications, allowing for rapid and reversible regulation of protein function[61–63]. Importantly, IDRs play a crucial role in driving the formation of biomolecular condensates, including P-bodies in the cytoplasm and nucleosomes in the nucleus through a

https://doi.org/10.1038/s41467-026-69183-9

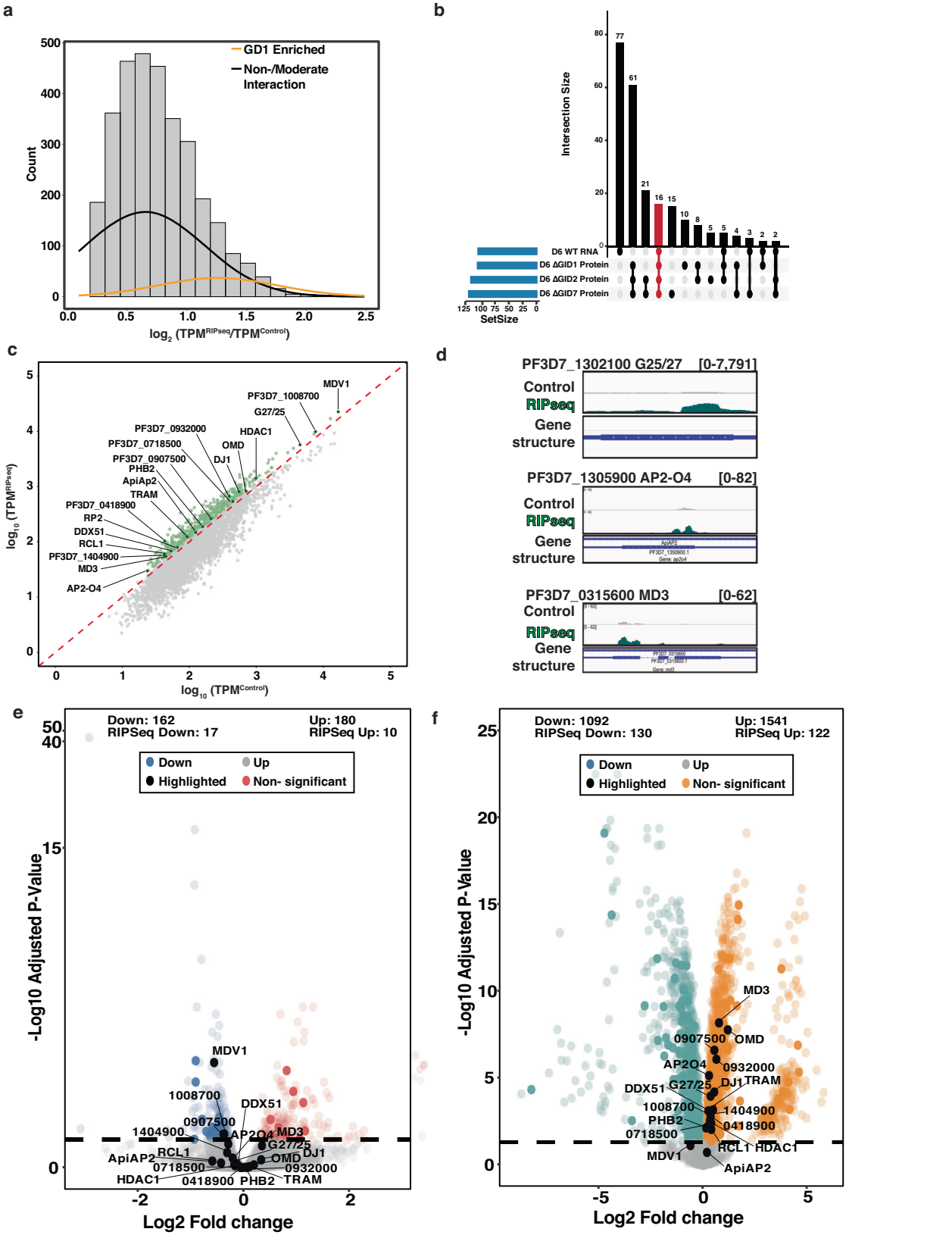

process called liquid-liquid phase separation[64]. In GD1, the IDRs may facilitate its dynamic interactions with mRNA and other P-body components, enabling swift assembly and disassembly of these regulatory hubs in response to cellular needs. This property could be crucial for forming and regulating P-bodies, which are membrane-less organelles that concentrate mRNAs and regulatory proteins. For PfDPL, the IDRs could mediate its association with nuclear condensates, promoting interactions with chromatin and co-transcriptional machinery, potentially allowing for quick changes in gene expression patterns during male gametocyte development. The targeted ubiquitination of these IDRs by PfGID represents a sophisticated mechanism for fine-tuning the levels and activities of these key regulatory proteins, potentially

Fig. 5 | The PfGID-GD1 axis controls the translational repression of key cell-fate molecules in gametocytes. a Log-transformed enrichment ratios of transcripts detected in GD1-HA day 6 gametocytes, modelled using two Gaussian distributions: broad non/moderate interaction group (black) and a highly enriched subset (orange). **b** UpSet plot showing the intersection of three defined transcript/protein sets:(i) GD1-bound transcripts identified by RIP-seq enrichment (LOD > 0); (ii) transcripts upregulated at day 6 relative to day 3, measured by RNA-seq; (iii) proteins upregulated in ΔPfGID parasites (ΔPfGID1, ΔPfGID2, or ΔPfGID7) at day 6 compared with parental controls. The red bar highlights the "potentially repressed" class: mRNAs that are bound by GD1 and whose protein products increase in abundance upon PfGID loss, consistent with translational de-repression in the absence of PfGID **c** Relative mRNA abundance in GD1-HA immunoprecipitates vs. input, with enrichment defined by the log of the odds (LOD) ratio from (Fig. 5a). Transcripts with LOD > 0 were considered highly enriched (green), while grey represents all others. Dark green colour and annotation highlight selective candidates linked to cell fate and gene regulation. **d** Representative transcripts showing varying enrichment levels after PfGD1-HA immunoprecipitation. Profiles depict total read counts per nucleotide in input (grey) and IP-enriched (green) samples, with paired tracks plotted on the same scale (denoted in brackets) for pfg25/27 (top), ap2-04 (middle) and md3 (bottom). **e** Volcano plot of day 6 vs. day 3 gametocytes iGP2 transcriptome identified by RNAseq. The distribution of GD1 RIP-Seq transcripts highlighted and potentially repressed proteins in black were analysed using two-sided *t* tests and adjusted with Benjamini–Hochberg FDR with *p*-value < 0.05, log2FC ≥ 0 (increased) or ≤ 0 (decreased). Data is from $n = 3$ biological replicates. **f** Volcano plot of differentially expressed proteins in ΔPfGID7 proteomes (day 6) vs. parental, with RIP-Seq transcript products highlighted and potentially repressed proteins in black. $n = 3$ per condition, Data analysed using two-sided *t* tests and adjusted with Benjamini–Hochberg FDR with *p*-value < 0.05, log2FC ≥ 0 (upregulated) or ≤ 0 (downregulated).

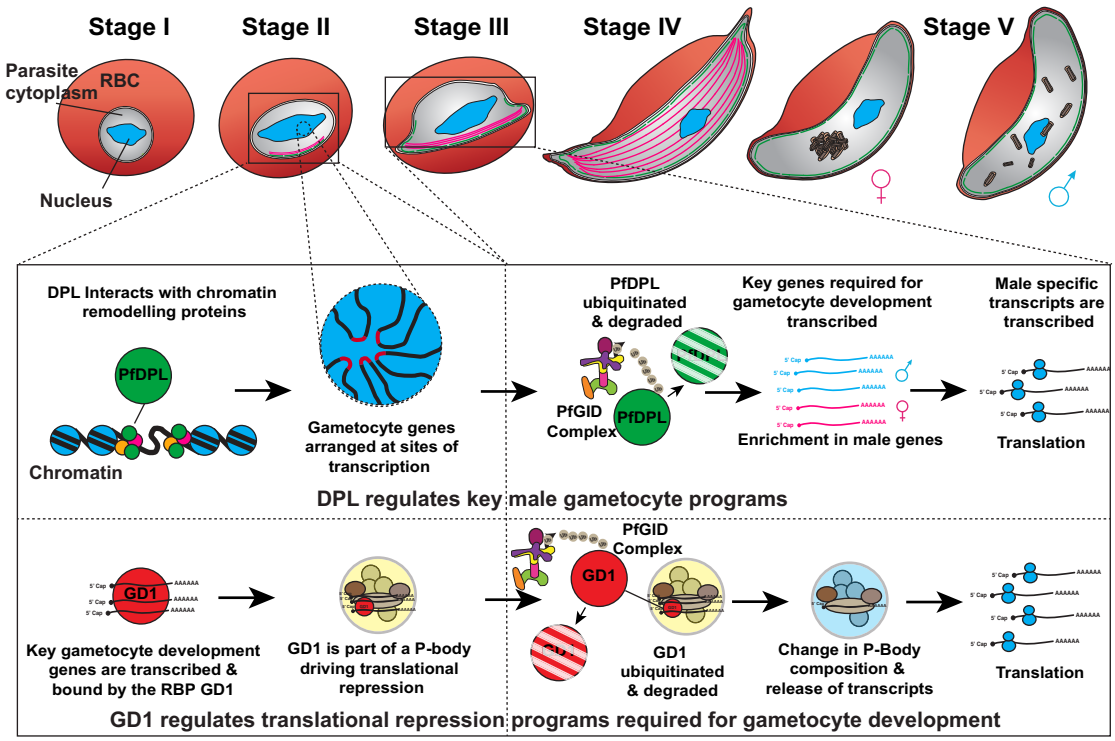

Fig. 6 | The E3 ubiquitin ligase PfGID regulates PfDPL and GD1 levels, controlling male and female gametocyte differentiation in *P. falciparum*. This model illustrates the function of the PfGID complex in regulating gametocyte development through the ubiquitination of PfDPL and GD1. The figure is divided into three panels. Top panel: Depicts gametocytogenesis from stage I to V, highlighting the sexual bifurcation into male and female gametocytes at stage IV. Middle panel: Illustrates the proposed function of PfDPL as a potential organiser of chromatin remodelling, facilitating the spatial organisation of gametocyte-specific genes at transcription sites. PfGID regulates PfDPL levels through ubiquitination, thereby controlling the activation of key genes essential for male gametocyte development. Bottom panel: Shows the role of GD1 in P-body formation and translational repression. PfGID modulates GD1 levels via ubiquitination, fine-tuning translational repression programmes crucial for gametocyte development. As GD1 levels decrease, P-body composition changes, leading to the release of transcripts for active translation, which drives the differentiation of gametocytes to stage V. This regulatory system, orchestrated by PfGID, ensures the precise temporal control of gene expression and protein levels required for successful gametocyte maturation and sexual stage progression in *P. falciparum*.

modulating their ability to form or participate in biomolecular condensates. This precise control may be crucial for the parasite's ability to coordinate the complex process of gametocytogenesis. Furthermore, the regulation of IDR-containing proteins by PfGID highlights the parasite's adaptation of a conserved eukaryotic regulatory strategy to meet the unique demands of its life cycle[65]. Future structural and functional studies of these IDRs could provide valuable insights into the specificity of PfGID-substrate interactions and the dynamics of P-body formation in *P. falciparum*.

Our data suggest that the PfGID complex, GD1, and PfDPL play recurring roles throughout *P. falciparum* development, with transcripts detected at multiple life cycle stages[66–68]. This multi-layered, temporally controlled regulation is reminiscent of developmental checkpoints in other eukaryotes[69] and may represent a conserved strategy for ensuring proper cellular differentiation across the parasite life cycle. The evolutionary conservation of the GID/CTLH complex not only underscores the importance of this regulatory mechanism but also provides insights into the molecular adaptations that have enabled Apicomplexan parasites to evolve and maintain their complex life cycles. This conserved regulatory system may have provided early branching eukaryotes with the flexibility to navigate diverse host environments and optimise their transmission strategies response to environmental cues and developmental signals[22].

In conclusion, our findings synergise with a recent study in *T. gondii*[17] and supports an emerging model of GID-mediated cell fate regulation in Apicomplexan parasites. We present evidence of a parasite-expressed component potentially linked to circadian rhythm governing male gametocyte development and an RNA-binding protein controlling P-body assembly and translational repression. Our data reveal a multi-dimensional understanding of malaria parasite development, integrating gene transcription control, translational repression, and ubiquitination. These insights not only advance our understanding of parasite biology but also open new avenues for targeted interventions in the ongoing fight against malaria.

Methods

Methods ethics statement

Use of human blood and serum was approved by the Walter and Eliza Hall Institute of Medical Research Human Ethics Committee under approval numbers 19-05VIC-13 and HREC21/6. All animal procedures were approved by the Walter and Eliza Hall Institute of Medical Research Animal Ethics Committee under approval numbers 2017.014 and 2019.013.

Parasite culture and transfection

Asexual blood stage cultures of *P. falciparum* were grown in O^+ erythrocytes (Lifeblood Australia) and maintained in Roswell Park Memorial Institute (RPMI) RPMI 1640 medium, Glutamax, HEPES (ThermoFisher) supplemented with 50 µg/ml hypoxanthine, 20 µg/ml gentamicin, 0.25% (w/v) Albumax II™ (ThermoFisher), and 5% (v/v) heat-inactivated human serum (Lifeblood, Australia. Agreement number 21-06VIC-01). The parasite cultures were maintained in microisolator boxes gassed with malaria gas mix (94% N_2, 1% O_2 and 5% CO_2) and grown at 37 °C. In this study, the inducible gametocyte producing (iGP2) parasite line was used as the parental line. To stop commitment to gametocyte production, the parasites were cultured in the presence of 2.5 mM D-(+)-glucosamine hydrochloride. Parasite lines containing the human dihydrofolate reductase (*hdhfr*) gene were maintained on media containing 5 nM WR99210 (WR) or blasticidin deaminase on 11 µM blasticidin S HCl (BSD). The parasitemia of the cultures were monitored by Giemsa-stained thin blood smears, viewed on a microscope at 1000 x magnification. Transfections were performed on late stage segmented schizonts[70]. The Lonza Amaxa Basic Parasite Nucleofector Kit 2 and Amaxa Nucleofector device was used for tranfections, using programme U-33. A full list of the cell lines generated in this study is shown in the Reagents and Resources table. If cell lines were shown to be non-clonal when generated, they were cloned by limiting dilution and individual clones were selected and verified.

Construction of the MGET-GFP reporter plasmid

To generate the MGET-GFP reporter line, we amplified the promoter region of the *mget* by PCR (PF3D7_1469900) from NF54 gDNA using the SL316/ SL317 oligonucleotides and cloned this fragment into the *Not*I/*Nhe*I restriction sites of the pkiwi003-p230p-bsfGFP plasmid[71] (Supplementary Data 1). The resulting pkiwi-*p230p-mget_pro*GFP plasmid was designed to be integrated into the *p230p* locus in the genome (PF3D7_0208900). As *p230p* is required for male gametocytes, we replaced the 5′ and 3′ homology sequences of *p230p* with sequences from the non-essential *pfs47* gene (PF3D7_1346800). The 5′ and 3′ homology arms of *Pfs47* were amplified from NF54 gDNA by PCR using the oligonucleotides SL360/ SL361 and SL362/ SL363, respectively and cloned sequentially into the *Xho*I/ *Hind*III and *Sac*I/ *Not*I restriction sites of the pkiwi-*p230pmget_pro*-GFP plasmid. The final plasmid pkiwi-*Pfs47-mget_pro*-GFP does not contain a drug selection cassette, allowing for marker-free cell lines.

Appropriate CRISPR-Cas9 guide sequences were selected using the online software CHOPCHOP[72]. To generate the CRISPR-Cas9 guide plasmid for targeting the *Pfs47* locus, the complementary guide oligonucleotides (SL364/ SL365) were annealed and Infusion cloned (Takara) into the pDC2-DHFR-Cas9-P230p plasmid, generating the pDC2-DHFR-Cas9-Pfs47. The *dhfr* coding sequence was replaced with the blasticidin S deaminase gene *(bsd)* to produce pDC2-BSD-Cas9-Pfs47 for use in cell lines that already had plasmids containing the *hdhfr* resistance cassette.

Integration of the repair templates into the *Pfs47* locus was verified by PCR using the SL 367/ SL346 and SL366/SL347 primers to test for integration and SL 366 and SL367 to test for the presence of wildtype locus. All oligonucleotide and plasmid sequences are detailed in Supplementary Table S1A, B.

All oligonucleotides used are listed in Supplementary Data 5.

Construction of the gene knockout plasmids

The ΔPfGID1, ΔPfGID2, ΔPfGID7, ΔPfGID8, ΔPfGID9, ΔPfYPEL5, ΔGD1, and ΔPfDPL gene knockout plasmids were created by modifying the p1.2-RON3-HA-mNeonGreen plasmid. The 5′ and 3′ homology regions (HR) were PCR amplified from NF54 gDNA using the oligonucleotides outlined in Supplementary Table S1A, and the fragments sequentially cloned into the *Not*I/ *Xma*I (5′ HR) and *Eco*RI/ *Kas*I (3′HR) restriction enzyme sites of the p1.2-RON3-HAmNeonGreen plasmid. The resulting gene KO plasmids were linearised and ready for transfection. This plasmid has a *hdhfr* drug selection cassette. A full list of the gene KO plasmids and sequences are shown in Supplementary Table S1B.

The CRISPR-Cas9 guide sequences were selected, annealed and inserted into the *Btg*ZI digested pUF1-Cas9G plasmid using InFusion cloning (Takara). The guide sequences used for each gene can be found in Supplementary Table S1 A. The full list of the KO cell lines generated, including the parent line used, is shown in the Reagent and Resource table. The deletion of the target locus was confirmed by PCR using gene and vector specific primers Supplementary Table S1 A.

All oligonucleotides used are list in Supplementary Data 5.

Construction of the epitope tagging plasmids

The PfGID1-HA, PfGID7-HA, PfGID8-HA, PfGID8-Flag-StrepII, PfGD1-HA-mScarlet and PfDPL-HA targeting plasmids were created by modifying the p1.2-RON3-HA-mNeonGreen plasmid. A synthetic gene sequence was designed that contained a region of homology followed by the remaining downstream coding sequence that had been recodoned (Genscript). This 5′ HR recdoned sequence was cloned into the *Not*I/ *Xma*I restriction enzyme sites of the p1.2RON3-HA-mNeonGreen plasmid. The 3′ homology regions for each construct were amplified by PCR from 3D7 gDNA and cloned in *Eco*RI/ *Kas*I sites of the plasmids. The p1.2 GID8Flag-StrepII and p1.2- GD1-HA-mScarlet plasmids were created by replacing the HAmNeonGreen and mNeonGreen sequence in the plasmid with synthesised sequences encoding for Flag-StrepII and mScarlet, respectively. The p1.2-GID8-HA, PfGID8-Flag-StrepII and GD1-HA-mScarlet vectors were further modified by replacement of the *dhfr* coding sequence with the blasticidin S deaminase gene *(bsd)*. Gene-specific guides were cloned into the pUF1Cas9G as described above.

For the creation of the GD1-overexpression plasmid, a synthetic gene consisting of recodoned full-length GD1-3xHA (Genscript) was cloned into the *Nhe*I/ *Pst*I sites of the pkiwi-*Pfs47mget_pro*-GFP plasmid described above. Next, the promoter sequence of the sexual stage-specific gene *Pfs16* (PF3D7_0406200) was amplified by PCR (oligonucleotides SL506/ SL508) and cloned into the *Sac*II/ *Nhe*I enzyme sites to create the pkiwi-Pfs47-*Pfs16_pro*GD1-3xHA plasmid.

The full list of oligonucleotides, and plasmid constructs can be found in Supplementary Data 5.

Gametocyte cultures and stage distribution assays

Cultures containing a majority ring stage iGP2 asexual parasites were sorbitol synchronised and returned to the culture at 3% parasitemia without glucosamine in the media to trigger gametocyte conversion

(day 2). The next day (day 1), the culture contained trophozoite and schizont stage parasites. The culture media was replaced with fresh media that did not contain glucosamine and placed in a shaking incubator set at 40 rpm overnight to reduce multiple infections in the culture. On day 0, gametocyte rings and asexual rings will be present. To remove asexual stage parasites, the culture media was supplemented with 62 mM N-acetyl-D glucosamine (NAG) for the remaining 12 days of development. Gametocyte development was monitored using microscopy of Giemsa-stained thin blood smears. Gametocyte morphology was visually scored based on previous criteria.

Stage distribution assays were established as described above, and smears were taken daily for the 12 days of the assay. Gametocyte stage was assessed from day 3 onwards by visually scoring the stage of 50–100 gametocytes chosen at random. The percentage of each life-cycle stage was then calculated, and the mean and standard error of the mean from three experiments were plotted.

Gametocyte parasitemia was assessed on day 6. The mean and the standard error of the mean from three experiments was plotted and significance tested by performing an ordinary one-way ANOVA test (Kruskal-Wallis test) in Graphpad Prism.

Gametocyte culture for transmission

Gametocyte cultures for transmission were initiated as described above and grown in RPMI 1640 medium, Glutamax, HEPES (ThermoFisher), supplemented with 50 µg/mL hypoxanthine and 10% (v/v) heat-inactivated human serum (Lifeblood, Australia). A total of 45 mL of culture was used and divided equally into each well of a six-well plate. The media was replaced daily from day 2 until day 12 using a slide warmer set to 37 °C to ensure the gametocytes remained warm. On day 12 of the gametocyte culture, the stage V gametocyte numbers were counted.

Exflagellation assays

A 50 µL sample of culture containing day 12 gametocytes was harvested and transferred to a 1.5 mL microcentrifuge tube. The microcentrifuge tube was kept at 37 °C to prevent premature activation. A 50 µL aliquot of pre-warmed ookinete medium (in RPMI 1640 medium, Glutamax, HEPES (ThermoFisher) supplemented with, 50 µg/mL hypoxanthine, 10% (v/v) heat-inactivated human serum (Lifeblood, Australia) and 100 µM xanthurenic acid) was then added to the microcentrifuge tube and mixed well with a pipette. The mixture was left at room temperature for 15 min and then transferred to the hemocytometer. The number of exflagellation centres and the number of red blood cells in the sample were then counted and expressed as a percentage of exflagellation centres[73]. Graphpad Prism was used to perform an ordinary one-way ANOVA test (Kruskal-Wallis test to determine significance).

Standard membrane feeding assays

Day 3 post-emergent female *Anopheles stephensi* mosquitoes were glucose starved for 2-3 h prior to performing standard membrane feeding assays. Between 30–40 mosquitoes were used for each cell line per experiment. Standard membrane feeding assays (SMFAs) were performed using glass water jacket feeders, with pre-stretched parafilm (Sigma-Aldrich) stretched across the large opening in the feeder. The feeder was plumbed into a circulating water bath set to 38 °C via plastic tubing, mounted on top of the mosquito cages and allowed to reach temperature.

While the feeder was warming, the blood meal was prepared by diluting the day 12 stage V gametocytes with uninfected red blood cells to obtain a 500 µL sample at 0.4% parasitemia. This infected red blood cells sample is then mixed with 500 µL of heat-inactivated human serum to obtain a 50% haematocrit solution. All steps are performed, ensuring the temperature of the blood meal does not drop below 37 °C. Immediately, the prepared blood meal was transferred into the glass feeder, and mosquitoes were allowed to feed for 45 minutes. The mosquitoes were left to rest after feeding for another 20-30 minutes. The mosquitoes were then knocked-down with CO_2, and the fully engorged mosquitoes were sorted into a clean container.

Midgut dissections and oocyst counts

Seven days post-bloodmeal, infected mosquitoes were anaesthetised by placing mosquitoes at 20 °C for 5 min and transferred into a Petri dish containing 80% ethanol. Mosquito midguts were dissected from each group and stained with 0.1% mercurochrome for 15 min before being mounted on a glass slide, and the oocysts per midgut were counted by microscopy. Experiments were performed three times. The number of oocysts per midgut and the percentage of midguts containing oocysts (prevalence) was recorded. The mean and standard error of the mean are plotted. Statistical significance was determined by performing an ordinary one-way ANOVA test (Kruskal-Wallis test) in Graphpad Prism.

Generation of Pfg377 antibodies

The sequence corresponding to amino acids 666 to 1146 of Pfg377[29] was subcloned into the pET-28a(+)-TEV plasmid to express an N-terminal His-tag followed by a TEV protease cleavage site. Pfg377 was expressed in *E. coli* BL21 (DE3) cells as an inclusion body and solubilised in 50 mM Tris pH 8, 6 M guanidine HCl. Pfg377 was purified via NiNTA agarose (Qiagen) resin, eluted in 10 mM Tris pH 4.5, 100 mM NaH_2PO_4, 8 M urea and then dialysed against 20 mM Tris pH 8, 20 mM NaCl. Soluble Pfg377 was further purified via a 1 mL HiTrap Q HP column (Cytiva) followed by size exclusion chromatography (S200 Increase 10/300 GL, Cytiva) pre-equilibrated in PBS. Polyclonal antibodies against Pfg377 (R2313) were generated in a rabbit at the WEHI Antibody Facility through three rounds of immunisation with recombinant Pfg377. All procedures were approved by the Walter and Eliza Hall Institute of Medical Research Animal Ethics Committee.

Fluorescence activated cell sorting (FACS) analysis assays

500ul of infected red blood cells (iRBC) were harvested by centrifugation at 500 x *g*, and the supernatant was discarded. The iRBC pellet was resuspended in 1:10000 Hoechst 33342 (ThermoFisher Scientific) in 1xDPBS. The sample was incubated in the dark at 37 °C for 30 min. The sample was centrifuged at 500 x *g*, the supernatant discarded, and the sample washed three times in 1 ml of DPBS. The samples were resuspended in 1 ml of DBPS and analysed for the presence of parasites using an LSR II Flow cytometer (Becton Dickinson). The (FACS) gating strategy is shown in Supplementary Fig. 8.

Immunofluorescence assays

Infected red blood cells (iRBC) were harvested by centrifugation at 500 x *g*, and the supernatant was discarded. The iRBC pellet was washed once in at least 10 volumes of 1 x DPBS, before being fixed in DPBS containing 4% (v/v) paraformaldehyde and 0.0075% (v/v) glutaraldehyde for 30 min at room temperature. The sample was centrifuged at 500 x *g*, the supernatant discarded, and the fixed iRBCs washed once in 5 volumes of DPBS. The fixed iRBCs were then permeabilised with 0.1% TX100 (v/v) in DPBS for 15 minutes and again centrifuged and washed. All antibody incubation steps were performed in 3% (w/v) BSA in DPBS. Rat α-HA (3F10), 1:300, Merck), rabbit α-Pfg377 (1:1000), rabbit α-GAP45 (R728, 1:1000)[74] and rabbit α-EXP2 (1:1000)[75] primary antibodies were incubated with the sample for 1- 2 h at room temperature, washed as described above and the secondary antibodies added to the iRBC and incubated for 1 hour. The native GFP and mScarlet fluorescence were visualised directly, without antibody labelling. goat α-rabbit IgG-conjugated Alexa fluor 488 or 594 (ThermoFisher) antibodies were used. After the secondary antibodies, the samples were stained with 2 µg/mL DAPI in PBS (ThermoFisher) for

10 min and washed a final time before a small sample of the iRBC pellet was placed on a glass slide and mounted under a coverslip and sealed with nail polish before proceeding to imaging.

A Leica Stellaris 8 confocal microscope equipped with a white light laser (WLL) and 405 nm diode laser was used to image the samples. DAPI was excited with the 405 nm diode laser, and wavelengths of 499 nm and 590 nm were selected to excite GFP and Alexa594, respectively. All images were acquired using a 1.4 NA 63x HC PL APO CS2 oil immersion objective. A consistent pixel size of 58 nm was set for all images to satisfy the optimal sampling. DAPI signal was collected on a HyD X detector over a range of 430-494 nm, GFP was collected on a HyD S over a range of 510 – 583 nm, and Alexa594 was collected on a HyD X over a range of 600-750 nm. Both HyD X detectors were operated in digital mode with a gain of 10 V, and the HyD S operated in analogue mode with a gain of 2.5 V. Z-stacks were set to capture a full parasite infected RBC with a system optimised sampling frequency. Between 40–50 parasites were imaged for each biological replicate, with single parasites imaged where possible to simplify the downstream analysis.

Image analysis

All images were analysed using a custom-written Fiji[76] macro to segment and quantify the mean fluorescence intensity in individual parasites. For all data with GAP45 labelling, the GAP45 channel was used for the mask creation for segmentation. For Pfg377 data, the mask was created using a summed image of both Pfg377 and MGET-GFP signals. For all data the masked channel was projected via a maximum intensity projection then had a gaussian blur, of radius 2, applied. This image was then auto-thresholded using a Li thresholding method before being converted to a mask. A fill holes binary operation was applied followed by three times erosion to account for uneven labelling across different parasites. Finally, a watershed separation was used to separate touching parasites. This mask was then used to measure the mean intensities of MGET-GFP, Pfg377 or GAP45 within the masked areas between the autothreshold values. Data were plotted for all conditions, normalised to the mean intensity for MGET-GFP parasites. All data were plotted using a web app for quantitative comparison of unpaired data[77].

Western blotting

Parasite cultures were harvested at the desired lifecycle stage, centrifuged at 500 x *g* and the supernatant discarded. Infected RBC pellets were then lysed with 5 pellet volumes of 0.03% saponin and incubated on ice for 15 min. The samples were centrifuged at 16,000 x *g*, the supernatants discarded, and the pellets washed 3 time with 1xPBS. The pellets were then resuspended in PBS containing Bolt LDS sample buffer and Bolt sample reducing agent (ThermoFisher). The samples were heated at 95 °C for 10 min and separated on 4–12% Bis-Tris gels (ThermoFisher) using 1 x MOPS buffer for 30 minutes. Gels were transferred to nitrocellulose membranes using the iBLOT 2 platform. Membranes were blocked in 3% skim milk (w/v) PBS for a minimum of 1 h prior to the addition of antibodies. Primary and secondary antibody dilutions were made in 3% (w/v) skim milk/PBS. Primary antibody incubations were performed either overnight at 4 °C or at room temperature for 1 h all secondary incubations were performed at room temperature for 1 h. The membranes were washed three times, 10 min each with PBS-Tween (PBS/0.05% (v/v) Tween 20) after antibody incubations. The following HRP-conjugated primary antibodies were used: mouse α-FlagM2-HRP conjugate (1:500, Merck) Rat α-HA-HRP conjugate (3F10, 1:300, Merck). A rabbit α -HSP 70 antibody (1:1000)[78] was used as a loading control and was detected using goat α-rabbit antibodies conjugated to HRP (1:1000, Merck). Blots were incubated with Biorad Clarity Western ECL substrate (Bio-Rad) for 5 minutes before being imaged on a ChemiDoc (Bio-Rad).

RNA sequencing

RNA was isolated from the PfGID1, 2, 7, 8 and 9 knockouts and parental iGP2 parasites at day 3, 6, 9 and 12 of gametocyte (five biological replicates for each cell line and time point were performed) development using the Isolate II RNA mini kit (Bioline). The RNA concentration of each sample was calculated using the QuantiFluor RNA system (Promega), and RNA quality was determined using high-sensitivity RNA screen tape analysis (Agilent). The RNA concentrations were then normalised to 1 ng/μL by dilution with the FlexDrop automated dispenser (Revvity), and then re-quantified. 1.1 ng of total RNA was reverse transcribed using SuperScript II (Invitrogen) and processed using an adapted CelSeq2 protocol. Briefly, barcoded samples with unique molecular identifiers (UMIs) were pooled after first- strand cDNA synthesis and second-strand synthesis performed using the MEGAscript T7 transcription kit (ThermoFisher). Amplified RNA was reverse transcribed using a tagged random hexamer without fragmentation, followed by sequencing on a NextSeq 2000 P3 flow cell (Illumina). Technical replicates were performed for each RNA sample.

RNA-seq analysis

RNA-seq reads were mapped to the *P. falciparum* reference genome (*P. falciparum* 3D7, PlasmoDB v66) and ERCC spike-in sequences using the Subread aligner (v2.16.0)[82] and assigned to genes using scPipe (v2.2.0)[79] with gene annotations also taken from the 3D7 *P. falciparum* reference genome (PlasmoDB v66). Gene counts were exported as UMI-level and read-level count matrices by scPipe. Following comparisons of the UMI-level and read-level data, the read-level data was used for subsequent analysis. All analyses were performed in R (v4.3.3)[80] using Bioconductor (v3.18), with differential expression analyse using edgeR (v4.0.1)[81] and limma (v3.58.1). Technical replicates with small library sizes were excluded (17 / 240 technical replicates with library size < 303,590 reads, corresponding to 3 median absolute deviations below the median on a log scale). Data from the remaining technical replicates were aggregated by summing the read-level counts to form $n = 116$ biological replicates with a median of 5,456,385 reads/sample. The 'filterByExpr' function from edgeR[82] was applied to determine which genes had sufficiently large counts to be retained in a differential expression analysis (5313 / 5687 genes), and library sizes were normalised using the trimmed mean of M-values (TMM) method was applied to determine which genes had sufficiently large counts to be retained in a differential expression analysis (5313 / 5687 genes), and library sizes were normalised using the trimmed mean of M-values (TMM) method[83].

The initial differential expression analyses used a design matrix consisted of a single factor specifying the 'cell line'-'timepoint' combination of each sample. The 'voomLmFit' function from edgeR[84,85] was used to transform count data to log2-counts per million (logCPM), estimate voom precision weights, estimate sample weights, and fit limma linear models while allowing for loss of residual degrees of freedom due to exact zeros. Samples were blocked by 'cell line replicate' to account for any correlation of the gene expression measurements taken from the same replicate over time, although the average correlation was low (0.02)[86]. Analysis conducted included comparisons of the same cell line between different days and different cell lines on the same day as required. In all comparisons, differentially expressed genes (DEGs) were defined as those with a Benjamini-Hochberg adjusted *P*-value < 0.05[87]. The results of the DE analyses were interactively explored using Glimma (v2.12.0)[88] and visualised as heatmaps using the pheatmap package (v1.0.12). The DEG lists and their gene ontology information are available in Supplementary Table S3 A-T., and fit limma linear models while allowing for loss of residual degrees of freedom due to exact zeros. Samples were blocked by 'cell line replicate' to account for any correlation of the gene expression measurements taken from the same replicate over time, although the average correlation was low (0.02)[86]. The DEG lists and

their gene ontology information are available in Supplementary Table S3 A-T.

Two types of gene set analyses were performed on the DEGs based on their gene ontology. Published transcript lists were used for these analyses and included lists of the top 100 male and female transcript lists[28] and lists of genes involved in translational repression and mRNA binding proteins[52]. The 'kegga' function from limma was used to perform over-representation analyses (i.e., hypergeometric test) of DEG lists, separately for up- and down-regulated DEGs. The 'cameraPR' function from limma was used to perform competitive gene set tests, accounting for inter-gene correlation, using the empirical Bayes moderated t-statistic. Heatmaps of the log-fold changes and 'barcode plots' of the empirical Bayes moderated t-statistics were used to visualise the expression of these genes in each comparison, while the 'fry' method was applied to perform a self-contained test of each gene set.

We also considered a time course analysis where the design matrix included the 'cell line' and their interactions with a cubic spline fit of 'timepoint' for each sample, again using the 'voomLmFit' function from edgeR with sample weights and blocking on 'cell line replicate'. Using this, we tested the following comparisons:

1. Any changes in gene expression over time (within cell line),
    a. ΔPfGID1KO, e.g.,
        i. Empirical Bayes moderated F-test of the coefficients ΔPfGID1:X1, ΔPfGID1:X2, and ΔPfGID1:X3, where X1, X2, and X3 are the 3 terms of the spline fit.
2. Any changes in gene expression over time in any of the KOs, i.e.,
    a. Empirical bayes moderated F-test of the coefficients ΔPfGID1:X1, ΔPfGID1:X2, ΔPfGID1:X3, ΔPfGID2:X1, ΔPfGID2:X2, ΔPfGID2:X3, ΔPfGID7:X1, ΔPfGID7:X2, ΔPfGID7:X3, ΔPfGID8:X1, ΔPfGID8:X2, ΔPfGID8:X3, ΔPfGID9:X1, ΔPfGID9:X2, and ΔPfGID9:X3, where X1, X2, and X3 are the 3 terms of the spline fit.

In all comparisons from the time course analysis, DEGs were defined as those with a

Benjamini-Hochberg adjusted P-value < 0.05[87]. The time course DEG lists are available in Supplementary Tables S3 A-T. The results of the time course DE analyses were visualised using customised plots made with ggplot2 (v3.4.4) as well as heatmaps made using the pheatmap package (v1.0.12). Owing to the complexities of grouping the resulting DEGs into 'similar' patterns, as compared to the simple 'up' or 'down' grouping in the non-time course DE analysis, no gene set tests were performed of the DEGs resulting from the time course analysis.

GD1 protein immuno-precipitation and RIP-Seq

Day 6 gametocytes from the GD1-HA parasite lines were harvested (three replicate experiments) and used to conduct RNA Immunoprecipitation Sequencing (RIP-Seq) to identify the mRNAs bound to GD1. For each replicate, two 30 mL culture dishes containing 5% gametocytes were harvested, and the media was discarded. The pellets were lysed in 0.15% (w/v) saponin in 1× Dulbecco's phosphate-buffered saline (DPBS) on ice for 15 minutes, before centrifugation at 16,000 x g for 5 minutes. The pellets were washed three times with 1x DPBS, with centrifugation at 16,000 x g for 5 min between washes. The washed pellets were then resuspended in 10 x the pellet volume of extraction buffer (1% NP-40 (ThermoFisher), 150 mM HEPES, and 150 mM NaCl (pH 7.0), supplemented with Complete

Protease Inhibitor Cocktail (Merck)). Samples were sonicated on ice using a Bandelin Sonoplus Sonicator UW3200 at 20% amplitude for 30 s, employing a 1 s on/off pulse cycle. Following sonication, samples were incubated overnight at 4 °C on a rotating platform. The next day, lysates were clarified by centrifugation at 16,000 x g for 20 min at 4 °C, and the resulting supernatant was collected for downstream processing.

Unenriched 'input' samples were prepared by reserving 10% of the starting lysate prior to immunoprecipitation, this sample acts as a control. The remaining lysate was subjected to immunoprecipitation (IP) by adding 20 µL of a-HA magnetic beads (Merck) to the cleared supernatant and incubating at 4 °C for 2 h with gentle rotation. Beads were then collected using a DynaMag-2 magnetic rack (ThermoFisher) and sequentially washed, five times with 1 mL of extraction buffer, five times with 1 mL of 0.5 x extraction buffer, and five times with 1 mL of nuclease-free water to reduce nonspecific binding.

For RNA extraction, 100 µL of the 'input' sample was mixed with 1 mL of TRIzol reagent (ThermoFisher). The immunoprecipitated RNA was extracted by directly resuspending the washed beads in 1 mL of TRIzol. Both the input and IP samples were then mixed with 200 µL of chloroform, vortexed, and centrifuged at 13,000 x g for 15 min at 4 °C to separate the aqueous phase. RNA was precipitated from the aqueous phase using isopropanol, and the RNA pellets were washed with 70% ethanol, air-dried, and resuspended in nuclease-free water for downstream processing. DNase treatment was performed using the Turbo DNA-Free DNase kit (ThermoFisher) following the manufacturer's protocol. DNA-free RNA quantification was performed using the Qubit 2.0 fluorimeter (ThermoFisher) using the High Sensitivity RNA reagent (ThermoFisher), and the RNA integrity was assessed on the 4100 Agilent Tapestation System using a High Sensitivity RNA kit.

Input and IP RNA sample libraries were generated using the Illumina Stranded Total RNA-seq Kit (Illumina), including the rRNA depletion. Final libraries were diluted in Nuclease-free water, and the library quality and integrity were assessed using a D5000 DNA kit on a 4100 Agilent Tapestation System (Agilent). Samples were run with 150 paired-end sequencing on the Miniseq platform (Illumina).

The quality of raw sequencing reads was assessed using FASTQC software with default settings. Low-quality reads were filtered and trimmed using Trimmomatic v0.39[89] applying a sliding window of 4 nucleotides, a minimum average PHRED64 quality score of 20, trimming of leading and trailing sequences by 3 nucleotides, and a minimum read length of 50 nucleotides. The resulting trimmed paired-end reads were then aligned to the *P. falciparum* 3D7 (PlasmoDB v68) genome using Subread[90] with default parameters. Gene-wise read counts were subsequently obtained using featureCounts[91] with the *P. falciparum* 3D7 68 GFF annotation file, applying the -S option to ensure strand specificity and enable accurate quantification of strand-specific reads. To identify enriched transcripts from RIP-Seq data, raw read counts were obtained from both RIP and control (input) samples and merged with transcript length information. Genes with low expression (≤ 5 reads in more than one replicate per condition) and low composite read coverage ($\sqrt{(RIP_1 \times RIP_2 \times RIP_3 + Control_1 \times Control_2 \times Control_3)} \leq 10$) were filtered out to ensure robust quantification. Transcript expression was normalised using Transcripts Per Million (TPM), and median TPM values were calculated for both RIP and control groups. Enrichment was determined as the $\log_2$-transformed ratio of median TPM values (RIP over control), with values constrained to finite numbers. A two-component Gaussian mixture model (GMM) was fitted to the $\log_2$ enrichment ratio distribution to classify transcripts as enriched or non-enriched based on the log odds ratio (LOD) of posterior probabilities. Transcripts with LOD > 0 were considered enriched. A histogram overlayed with GMM component density curves visualised the enrichment distribution, while a $\log_{10}$-scaled TPM scatter plot highlighted select transcripts of interest. All data processing and visualisation were performed using R with the ggplot2, mixtools, and ggrepel packages. Gene ontology enrichment for the RIP-Seq enriched genes was performed using STRING v12. We visualised interaction networks at a medium confidence score of 0.4, with continuous lines for direct interactions and dashed lines for indirect associations and

clustered the network using the Markov Cluster Algorithm with a default inflation score of 3.

Enrichment analysis was run in STRING v12.0 (string-db.org) using the built-in Reactome and Gene Ontology (Biological Process) libraries. The background was the organism-wide *Plasmodium falciparum* 3D7 proteome. P values were adjusted by Benjamini–Hochberg; terms with FDR (q) < 0.05 were retained. STRING's "Strength" reported in the figures is log10(observed/expected) enrichment. For all analyses, study gene lists (PlasmoDB/3D7 identifiers) were mapped to STRING with the default resolver; duplicate mappings were collapsed and unmapped IDs excluded. Protein–protein interaction (PPI) networks used the default evidence channels with a medium confidence threshold (combined score ≥ 0.4); disconnected nodes were hidden, and networks were laid out on STRING's two-dimensional force-directed coordinates and exported for clustering. Clustering was performed as follows: for the GID–RIP-Seq PPI network, modules were defined with the Markov Cluster Algorithm (MCL; inflation = 3); for all other STRING networks in the main and extended figures including PPI maps and the term–term similarity graphs underlying enrichment maps and modules were defined with DBSCAN (density-based spatial clustering of applications with noise) applied to the exported 2D coordinates using default ε and minPts, allowing sparse nodes to remain unassigned (noise). For visualisation, the enriched terms are shown as a monochrome lollipop/bubble plot where the size of the circle area equales gene count and the x-axis is the STRING "Strength"; PPI maps display node size by degree, edge thickness by combined score, and module boundaries by the assigned MCL (GID–RIP-Seq only) or DBSCAN (all others) clusters.

To identify if GD1-associated transcripts were translationally repressed, we integrated transcriptomic (RNA-Seq) and proteomic datasets from day 6 wild-type and ΔPfGID knockout (KO) gametocytes, focusing on genes with robust mRNA levels (up-regulated or stable transcript level) but low protein abundance that become significantly up-regulated at the protein level in the ΔPfGID.

Immunoprecipitation assays

Five biological replicates were performed for each parasite line and condition. For each replicate, 3 × 30 mL dishes of cultures at 5–10% parasitemia were harvested by centrifugation at 500 x *g*, and the resulting pellets were lysed using 0.15% (w/v) saponin in 1 x DPBS). Following lysis with saponin, the iRBC pellets were washed three times in DPBS, with centrifugation at 16,000 x *g* between washes. These pellets were then incubated with 10x the pellet volume of extraction buffer (1% NP40 (Thermo Fisher Scientific), 150 mM HEPES, 150 mM NaCl, pH 7) supplemented with Complete Protease Inhibitors (Merck). These samples were then sonicated on ice using a Bandelin Sonoplus Sonicator UW3200 with pulses set at 20% amplitude for 30 s with a 1 s on/off cycle. The sonicated samples were incubated overnight on a roller at 4 °C. The samples were centrifuged at 16,000 x *g* for 20 min, and the supernatant was collected. 20 µL of anti-HA magnetic beads (Merck SAE0197-1ML) were added to the supernatant and allowed to bind at 4 °C for 2 h. Beads were collected using a DynaMag2 magnetic rack and washed 5 times with 1 mL of extraction buffer, followed by five 1 mL washes of H_20 water. Protein was eluted from the beads by adding 150 mL of 0.5% (w/v) SDS in H_20 prewarmed to 95 °C and incubated on the beads for 2 min. Samples were either examined by western blotting or mass spectrometry.

Sample preparation of IP samples for mass spectrometry analysis

Eluates from immunoprecipitations were prepared for LC-MS/MS analysis using the Filter Assisted Sample Preparation (FASP) method[92] with the following modifications. Briefly, eluates were added to a Vivacon® 30 kDa MWCO (Sartorius, VN01H22), and proteins were solubilised and reduced in 6 M urea (Wako, Japan) containing 10 mM Tris-(2carboxyethyl)phosphine (TCEP, Sigma-Aldrich) for 30 min, alkylated with 50 mM iodoacetamide (Sigma-Aldrich), then digested with 1 µg trypsin (SoLuTrypsin, Sigma Aldrich) in 50 mM ammonium bicarbonate (AmBic) (Sigma-Aldrich) and incubated overnight at 37 °C. Peptides were eluted with 50 mM AmBic in two 40 µL sequential washes and acidified in 1% formic acid (FA, final concentration). Peptides were lyophilised to dryness using a CentriVap (Labconco) before being reconstituted in 30 µL of 0.1% formic Acid (FA)/2% acetonitrile (ACN), ready for mass spectrometry analysis.

Sample preparation for mass spectrometry-based global proteomics analysis

Five biological replicates were performed for each parasite line and condition. Saponin lysed infected RBC pellets were lysed in 100 µL of preheated (95 °C) buffer (2.5% SDS in 100 mM Tris-HCl, pH 8.5). DNA was hydrolysed by adding 2 µL neat Trifluoroacetic acid (TFA) (Sigma), and lysates were neutralised to pH 8.5 by adding 40 µL of 1 M Tris-HCl. Protein concentration was determined using Pierce™ BCA Protein Assay Kit following the manufacturer's instructions. Cell lysates (20 µg protein per replicate) were transferred to 0.5 mL LoBind Deep Well plate (Eppendorf) prepared for mass spectrometry analysis using the modified SP3 protocol[93] with some modifications. Briefly, samples were subjected to simultaneous reduction and alkylation with a final concentration of 10 mM Tris (2carboxyethyl) phosphine (TCEP) and 40 mM 2-chloracetamide followed by heating at 95 °C for 10 min. Prewashed magnetic PureCube Carboxy agarose beads (20 µl, Cube Biotech) were added to all the samples along with acetonitrile (ACN,70% v/v final concentration) and incubated at room temperature for 20 min. Samples were placed on a magnetic rack, the supernatants discarded, and the beads were washed twice with 70% ethanol and once with neat ACN. ACN was evaporated entirely from the tubes using a CentriVap (Labconco) before the addition of digestion buffer (50 mM Tris-HCl, pH 8) containing 1 µg each of enzymes Lys-C (Wako, 129–02541) and SOLu-Trypsin (Sigma-Aldrich, EMS0004). Trypsin-LysC on-bead digestion was performed with agitation (400 rpm) for 1 h at 37 °C on a ThermoMixer C (Eppendorf). Following digestion, the samples were transferred to pre-equilibrated AttractSPE tips C18 (Tips-C18.T3.200.96 AFF, Affinisep) for sample clean-up. The eluates were lyophilised before being reconstituted in 0.1% FA/2% ACN, ready for mass spectrometry analysis.

DDA-based mass spectrometry analysis of IPs and global samples

Reconstituted peptides (IPs: IGP2, GID8 and DiCre.WT, DiCre.WT.Rapamycin, HA.DPL, HA.DPL.Rapamycin) were run in a data-dependent (DDA) mode on an Orbitrap Eclipse™ Tribrid mass spectrometer interfaced with a Neo Vanquish UHPLC System. Peptides were loaded onto a C18 fused silica column (inner diameter 75 µm, OD 360 µm × 15 cm length, 1.6 µm C18 beads) with an integrated emitter tip (IonOpticks) using pressure-controlled loading with a maximum pressure of 1500 bar and an EASY-nLC source and electrospraying directly into the mass spectrometer. We then employed a linear gradient of 3% to 30% of solvent-B at 400 nl/min flow rate (solvent-B: 80% (by vol) acetonitrile) for 20 min and 30% to 40% solvent-B for 10 min and 35% to 99% solvent-B for 5 min which was maintained at 90% B for 10 min and equilibrated the column high pressure for 2 min comprising a total of 45 min run with a 30 min gradient in a data dependent (DDA) mode. MS1 spectra were acquired in the Orbitrap (R = 120 k; normalised AGC target = standard; MaxIT = Auto; RF Lens = 30%; scan range = 350–1500; profile data). Dynamic exclusion was employed for 30 s, excluding all charge states for a given precursor. Data-dependent MS2 spectra were collected in the Orbitrap for precursors with charge states 2-7 (R = 30k; HCD collision energy mode = fixed; normalised HCD collision energies = 30%; scan range first mass = 120 m/z; normalised AGC target = 200%; MaxIT = 45 ms).

DIA-based mass spectrometry analysis of IPs and global samples

Reconstituted peptides (IPs: CPSF, DiCre, GID7; Global: WT, GID1, GID2, GID8 and GID9) were separated by reverse-phase liquid chromatography on a 15 cm C18 fused silica column with an integrated emitter tip (IonOpticks, ID 75 μm, OD 360 μm, 1.6 μm C18 beads) using a custom nano-flow HPLC system (Thermo Ultimate 300 RSLC Nano-LC, PAL systems CTC autosampler). The HPLC was coupled to a timsTOF Pro (Bruker) equipped with a CaptiveSpray source. Peptides were loaded directly onto the column at a flow rate of 600 nL/min with buffer A (99.9% Milli-Q water, 0.1% FA) and eluted at 400 nL/min on a 30 min linear analytical gradient of increasing buffer B (90% ACN, 0.1% FA) from 2 to 34%. The timsTOF Pro (Bruker) was operated in diaPASEF mode using Compass Hystar 5.1. The settings on the TIMS analyser were as follows: Lock Duty Cycle to 100% with equal accumulation and ramp times of 100 ms, and 1/K0 Start 0.6 V.·/cm2 End 1.6 V·s/cm2, Capillary Voltage 1400 V, Dry Gas 3 l/min, Dry Temp 180 °C. The DIA methods were set up using the instrument firmware (timsTOF control 2.0.18.0) for data-independent isolation of multiple precursor windows within a single TIMS scan. The method included two windows in each diaPASEF scan, with window placement overlapping the diagonal scan line for doubly and triply charged peptides in the m/z – ion mobility plane across 16 × 25 m/z precursor isolation windows (resulting in 32 windows) defined from m/z 400 to 1200, with 1 Da overlap, and CID collision energy ramped stepwise from 20 eV at 0.8 V·s/cm2 to 59 eV at 1.3 V·s/cm2.

Reconstituted peptides (IPs: WT, HA-tagged and WT, GD1-HA in WT cells, GD1-HA in GID7KO cells and global proteomics: IGP, GID1, GID2, GID7) were separated using reverse-phase liquid chromatography on a 15 cm C18 fused silica column with an integrated emitter tip (IonOpticks, ID 75 μm, OD 360 μm, 1.6 μm C18 beads) using a nano-flow HPLC system (Thermo Ultimate 3000 RSLC Nano-LC) that is coupled to a Orbitrap Eclipse Tribrid Mass Spectrometer (Thermo Scientific) using Easy nLC source and electro sprayed directly into the mass spectrometer. Peptides were loaded directly onto the column at a flow rate of 600 nL/min with buffer A (99.9% Milli-Q water, 0.1% FA) and eluted at 400 nL/min on a 30 min linear analytical gradient of increasing buffer B (90% ACN, 0.1% FA) from 2 to 34%. Data was acquired in a data-independent (DIA) mode. MS1 spectra were acquired in the Orbitrap (R = 120 k; normalised AGC target = 300%; MaxIT = custom; RF Lens = 40%; scan range = 375–1500; profile data). Dynamic exclusion was employed for 30 s, excluding all charge states for a given precursor. MS2 spectra were collected in the Orbitrap (R = 30k; first mass = 120 m/z; normalised AGC target = 100%; MaxIT = 54 ms).

Reconstituted peptides (global proteomics: WT, GD1.KO and IGP2.WT, ΔDPL) were separated using reverse-phase liquid chromatography on a 15 cm C18 fused silica column with an integrated emitter tip (IonOpticks, ID 75 μm, OD 360 μm, 1.6 μm C18 beads) on a Neo Vanquish HPLC system coupled to a Thermo Fisher Orbitrap Astral. Peptides were analysed on a 25 min linear analytical gradient of increasing buffer B (80% ACN, 0.1% FA) from 2 to 34%. Data was acquired in a data-independent (DIA) mode. The MS1 settings were as follows: Orbitrap resolution 240,000; scan range m/z 380–980; AGC target 500%. The DIA parameters were as follows: isolation window: custom; HCD collision energy: 25%; scan range: m/z 145–1450; maximum injection time: 3 ms; AGC target: 800%.

Data processing and statistical analysis

Raw DDA MS data (IPs: IGP2, GID8 and DiCre.WT, DiCre.WT.Rapamycin, HA.DPL and HA.DPL.Rapamycin) were searched using MaxQuant 2.0.1.0, incorporating the Andromeda search engine[94]. The analysis was conducted against the *P. falciparum* 3D7 Reference proteome FASTA database obtained from UniProt (October 2021) and a separate reverse decoy database using a strict trypsin specificity, allowing up to 2 missed cleavages. The minimum required peptide length was set to 8 amino acids. Modifications: Carbamidomethylation of Cys was set as a fixed modification, while N-acetylation of proteins and oxidation of Met were set as variable modifications. First search peptide tolerance was set at 20 ppm, and main search set at 20 ppm (other settings left as default). Maximum peptide mass [Da] was set at 4600. The "match between runs" option in MaxQuant was used to transfer identifications made between runs based on matching precursors with high mass accuracy. Peptide-spectrum match and protein identifications were filtered using a target-decoy approach at an FDR of 1%. Label-free quantification (LFQ) quantification was selected, with a minimum ratio count of 2. Peptide-spectrum match scores and protein identifications were filtered using a target-decoy approach at an FDR of 1%.

Raw DIA data (IPs: CPSF, DiCre, GID7 and WT, HA-tagged and WT, GD1-HA (in WT cells) and GD1-HA (in GID7KO cells) and global proteomics: WT, GID1, GID2, GID8, GID9 and IGP, GID1, GID2, GID7) were analysed using DIA-NN 1.8[95] in library-free mode. diaPASEF acquired files were searched against reviewed sequences from *P. falciparum* 3D7 Reference proteome obtained from Uniprot (October 2021) with the following settings: trypsin specificity, peptide length of 7–30 residues, cysteine carbidomethylation as a fixed modification, variable modifications set to N-terminal protein acetylation and oxidation of methionine, the maximum number of missed cleavages at 1. Mass accuracy was set to 10 ppm for both MS1 and MS2 spectra and match between runs (MBR) enabled, and filtering outputs set at a precursor q-value < 1%.

Raw DIA data (global proteomics: WT, GD1.KO and IGP2.WT, ΔDPL) were analysed on Spectronaut version 19.2[96] using BGS factory settings of direct DIA analysis. A combined Human and *P. falciparum* Uniprot reference proteome (2021) was used for database searching.

All information relating to immuno-precipitation and global proteomics are available in Supplementary Data 6.

Data processing and statistical analysis of IPs

Data processing and statistical analyses were performed in R (v 4.2.0 - v4.4.0). Protein groups flagged as false hits, contaminants, reverse sequences, or 'only identified by site' were removed. Protein quantitative intensities were log2-transformed prior to downstream processing. Data quality was assessed by inspecting global log-intensity distributions, the number of detected precursors and proteins per sample and the extent and pattern of missing values. Sample-level structure and potential technical effects were further evaluated using principal component analysis (PCA) and relative log expression (RLE) diagnostics. Proteins were then filtered to retain those quantified in at least 60% of samples within at least one experimental group.

To reduce systematic technical variation, intensities were normalised across samples using cyclic loess normalisation implemented in limma (v3.60.4). Because the IP control and treated groups exhibited markedly different global abundance profiles, cyclic loess normalisation was performed within experimental groups to avoid borrowing information across conditions. No missing-value imputation was performed except for two experiments (IPs: CPSF, DiCre, GID7 and WT, HA-tagged) where missing values were imputed by applying the Barycenter approach (v2-MNAR) implemented in msImpute (v.1.7.0).

Statistical analyses comprised differential abundance testing for pairwise contrasts and multi-group comparisons (ANOVA framework) using limma. For differential analyses, linear models were fitted and moderated using empirical Bayes shrinkage, and p-values were adjusted for multiple testing using the Benjamini–Hochberg false discovery rate (FDR) procedure, with proteins considered significant at FDR-adjusted p-value < 0.05. Visualisations were generated in R, including volcano plots using ggplot2 (v3.5.1), heatmaps using pheatmap (v1.0.12), and UpSet plots using ComplexUpset (v1.3.3).

Data processing and statistical analysis of global proteomics

Data processing and statistical analyses were performed in R (v 4.2.1 - v4.4.2). Proteins lacking proteotypic precursors and those with *q*-values > 0.01 were excluded. Protein quantitative intensities were log2-transformed prior to downstream processing. Data quality was assessed by inspecting global log-intensity distributions, the number of detected precursors and proteins per sample and the extent and pattern of missing values. Sample-level structure and potential technical effects were further evaluated using principal component analysis (PCA) and relative log expression (RLE) diagnostics. Proteins were then filtered to retain those quantified in at least 60% of samples within at least one experimental group. To reduce systematic technical variation, intensities were normalised across samples (please refer to supplementary Data X for the normalisation strategy implemented in limma). No missing-value imputation was performed for most studies except for one (WT, GID1, GID2, GID8 and GID9) where missing values were imputed by applying Barycenter approach (v2-MNAR) implemented in msImpute (v.1.7.0).

Statistical analyses comprised (i) global longitudinal/trajectory modelling using maSigPro (v1.78.0), where applicable, (ii) unsupervised hierarchical clustering (hclust) to group proteins by similarity in their longitudinal trajectories over time, and (iii) differential abundance testing for pairwise contrasts and multi-group comparisons (ANOVA framework) using limma. Statistical analyses comprised differential abundance testing for pairwise contrasts and multi-group comparisons (ANOVA framework) using limma (v3.52.4). For differential analyses, linear models were fitted and moderated using empirical Bayes shrinkage, and p-values were adjusted for multiple testing using the Benjamini–Hochberg false discovery rate (FDR) procedure, with proteins considered significant at FDR-adjusted *p*-value < 0.05. Visualisations were generated in R, including volcano plots using ggplot2 (v3.5.2), heatmaps using pheatmap (v1.0.12), and UpSet plots using ComplexUpset (v1.3.3). A barcode enrichment plot was generated to visualise the distribution of a predefined protein set along the ranked differential-expression statistic (moderated t-statistics from limma), with the running enrichment curve computed using the barcodeplot function implemented in limma.

Protein extraction and digestion of samples for K-GG analysis

Five biological replicates were performed for each parasite line and condition, with parental iGP2 parasites used as a control. Saponin-isolated parasites were pelleted and snap frozen. Protein extraction was performed by adding pre-heated SDC buffer (1% sodium deoxycholate (SDC), 10 mM tris(2-carboxyethyl)phosphine (TCEP), 40 mM chloroacetamide (CAA), 75 mM Tris-HCl at pH = 8.5) to isolated-parasite pellets, resuspended and heated at 85 °C for 10 min. Samples were allowed to cool to room temperature before the addition of universal nuclease (ThermoFisher) and incubated for 5 minutes before centrifugation, and the clarified lysates were collected. Protein concentrations were determined using the BCA assay, and proteins were digested with trypsin/Lys-C mix overnight at 37 °C with a 1:50 enzyme to protein ratio. The digestion was stopped by adding three volumes of 1% trifluoroacetic acid (TFA) in isopropanol and loaded onto SDB-RPS cartridges (Strata™-X-C, 100 mg, Phenomenex Inc.). Columns were activated and pre-equilibrated with 3 mL of 30% methanol (MeOH)/1% TFA and washed with 3 mL of 0.2% TFA. Samples were loaded and washed twice with 3 mL 1% TFA in isopropanol and once with 3 mL 0.2% TFA/2% acetonitrile (ACN). Peptides were eluted twice with 2 mL of 1.25% ammonium hydroxide (NH_4OH)/80% ACN and diluted with water to a final ACN concentration of 30%. The eluates were snap-frozen in liquid nitrogen and lyophilised overnight.

Crosslinking of K-GG antibody

The kGG antibody—licensed to Cell Signalling Technology (PTMScan Ubiquitin Remnant Motif (K-epsilon-GG) Kit #5562) —bound beads were washed three times with 100 mM sodium tetraborate (pH 9.0) and then crosslinked for 30 minutes at room temperature with 0.5 mL of 20 mM dimethylpimelimate in 100 mM sodium borate (pH = 9.0). The cross-linking reaction was then quenched by adding 200 mM ethanolamine (pH = 8.0) and washed twice before being incubated for 2 h after the addition of 200 mM ethanolamine (pH = 8.0). The beads were washed three times with IAP buffer (50 mM MOPS, pH 7.2, 10 mM Na_2HPO_4, 50 mM NaCl).

K-GG peptide enrichment and LC-MS/MS sample preparation

K-GG peptides were resuspended in 0.5 ml of cold IAP buffer (50 mM MOPS pH 7.2, 10 mM Na2HPO4, 50 mM NaCl) and incubated with 2.5 μL of packed cross-linked K-GG antibody-bead conjugate (corresponding to 31 μg of antibody per sample) for 2 h at 4 °C with end-over-end rotation. Beads were transferred to glass-fibre filter stage tips and washed twice with 1 mL of IAP buffer and three times with cold water via centrifugation between each wash.K-GG peptide. The glass-fibre filter stage tips were then stacked onto SDB-RPS stage tips. The SDB-RPS stage tips were preactivated and equilibrated with the addition of 60 μL of isopropanol, 60 μL 80% ACN and 100 μL 0.2% TFA with centrifugation occurring between each addition.

The kGG peptides were eluted off the beads and directly captured onto the SDB-RPS stage tips via two separate TFA (100 μL of 0.15 %) elution and centrifugation steps. Peptides were then desalted by washing the SDB-RPS stage tips with 0.2% TFA/2% ACN, prior to elution with 60 μL 80% ACN/2.5% NH_4OH directly into level 3 SureStart 0.2 mL mass spectrometry vials (ThermoFisher). Peptides were Speedvac dried, resuspended in 10 μL of 0.1% FA/ 2% CAN and 4 μL injected into the mass spectrometer.

LC-MS/MS measurements of k-GG peptides

Peptides were loaded on a 25 cm IonOpticks column, which was maintained at 50 °C using a column oven. A Neo Vanquish UHPLC system (ThermoFisher) was directly coupled online with the mass spectrometer (Eclipse ThermoFisher), and peptides were separated with a binary buffer system of buffer A (0.1% formic acid (FA)) and buffer B (99.9% acetonitrile plus 0.1% FA), at a flow rate of 400 nL/minute. The gradient started at 2% B and increased to 34% in 48 min before increasing to 60% within 5 min and then reaching 90% in 1 min and held for 5 min prior to returning to 2% and re-equilibrated. The mass spectrometer was operated in positive polarity mode with a capillary temperature of 275 °C.

The DIA methods consisted of an MS1 scan (m/z = 350-1650) with an AGC target of 2.6×10^6 and a maximum injection time of 60 ms (R = 120,000). DIA scans were acquired at R = 30,000, with an AGC target of 3×10^5, "auto" for injection time and a default charge state of 3. The spectra were recorded in profile mode, and the stepped collision energy was 25, 27.5, 30% normalised collision energy. 38 non-uniform DIA segments were set to achieve an average of 6 data points per peak.

Raw data processing and analysis of k-GG peptides

MS raw files were processed using DIA-NN 1.8.1. Library-free searching with kGG variable modification enabled with a maximum of two modifications and two-missed cleavages was performed with the *P. falciparum* 3D7 proteome (Uniprot UP000001450), with MBR enabled and Robust LC quantification.

Precursors were averaged and filtered to retain kGG peptides that were observed in at least 3/5 biological replicates for at least one condition. Peptide intensities variance-stabilisation normalised, imputed using a mixed MLE/MinProb approach and limma differential expression analysis performed using the DEP R package. Significance testing of log2-transformed intensities was performed, and Benjamini-Hochberg corrected *p*-values < 0.01 were considered significant. All raw data files were uploaded to the PRIDE data repository as described above.

Statistical analysis
The computational and statistical analyses were executed using the specified open-source software tools in conjunction with the outlined procedures.

Reporting summary
Further information on research design is available in the Nature Portfolio Reporting Summary linked to this article.

Data availability
All biological data associated with this study are available in the Source data files and Supplementary Information. Biological tools generated in this study are available from the corresponding authors upon request. Proteomics data have been deposited to the ProteomeXchange Consortium via the PRIDE partner repository under accession code PXD048861. Mini-bulk RNA-seq data have been deposited in the NCBI-GEO database under accession GSE314126. Source data are provided in this paper.

Code availability
All scripts used in the processing and analysis of the RNA-seq data are available from https://github.com/WEHISCORE/G000396_Danu (Accession ID: https://doi.org/10.5281/zenodo.17957732.

References

1. Kafsack, B. F. et al. A transcriptional switch underlies commitment to sexual development in malaria parasites. *Nature* **507**, 248–252 (2014).
2. Sinha, A. et al. A cascade of DNA-binding proteins for sexual commitment and development in *Plasmodium*. *Nature* **507**, 253–257 (2014).
3. Venugopal, K., Hentzschel, F., Valkiunas, G. & Marti, M. *Plasmodium* asexual growth and sexual development in the haematopoietic niche of the host. *Nat. Rev. Microbiol.* **18**, 177–189 (2020).
4. Voss, T. S. & Brancucci, N. M. Regulation of sexual commitment in malaria parasites - a complex affair. *Curr. Opin. Microbiol.* **79**, 102469 (2024).
5. Hollin, T. et al. Proteome-Wide Identification of RNA-dependent proteins and an emerging role for RNAs in *Plasmodium falciparum* protein complexes. *Nat. Commun.* **15**, 1365 (2024).
6. Reddy, B. P. et al. A bioinformatic survey of RNA-binding proteins in *Plasmodium*. *BMC Genom.* **16**, 890 (2015).
7. Vembar, S. S., Droll, D. & Scherf, A. Translational regulation in blood stages of the malaria parasite *Plasmodium* spp.: systems-wide studies pave the way. *Wiley Interdiscip. Rev. RNA* **7**, 772–792 (2016).
8. Mair, G. R. et al. Regulation of sexual development of *Plasmodium* by translational repression. *Science* **313**, 667–669 (2006).
9. Mair, G. R. et al. Universal features of post-transcriptional gene regulation are critical for *Plasmodium* zygote development. *PLoS Pathog.* **6**, e1000767 (2010).
10. Shrestha, S., Li, X., Ning, G., Miao, J. & Cui, L. The RNA-binding protein Puf1 functions in the maintenance of gametocytes in *Plasmodium falciparum*. *J. Cell Sci.* **129**, 3144–3152 (2016).
11. Miao, J. et al. Puf mediates translation repression of transmission-blocking vaccine candidates in malaria parasites. *PLoS Pathog.* **9**, e1003268 (2013).
12. Chene, A. et al. PfAlbas constitute a new eukaryotic DNA/RNA-binding protein family in malaria parasites. *Nucleic Acids Res.* **40**, 3066–3077 (2012).
13. Hart, K. J. et al. *Plasmodium* male gametocyte development and transmission are critically regulated by the two putative deadenylases of the CAF1/CCR4/NOT complex. *PLoS Pathog.* **15**, e1007164 (2019).
14. Balu, B. et al. CCR4-associated factor 1 coordinates the expression of *Plasmodium falciparum* egress and invasion proteins. *Eukaryot. Cell* **10**, 1257–1263 (2011).
15. Russell, A. J. C. et al. Regulators of male and female sexual development are critical for the transmission of a malaria parasite. *Cell Host Microbe* **31**, 305–319 e310 (2023).
16. Ponts, N. et al. Deciphering the ubiquitin-mediated pathway in apicomplexan parasites: a potential strategy to interfere with parasite virulence. *PLoS ONE* **3**, e2386 (2008).
17. Uboldi, A. D. et al. Differentiation of *Toxoplasma* into latent forms is linked to central carbon metabolism and requires a GID/CTLH-type E3 ubiquitin ligase. Preprint at https://doi.org/10.1101/2025.07.27.667068 (2025).
18. Santt, O. et al. The yeast GID complex, a novel ubiquitin ligase (E3) involved in the regulation of carbohydrate metabolism. *Mol. Biol. Cell* **19**, 3323–3333 (2008).
19. Francis, O., Han, F. & Adams, J. C. Molecular phylogeny of a RING E3 ubiquitin ligase, conserved in eukaryotic cells and dominated by homologous components, the muskelin/RanBPM/CTLH complex. *PLoS ONE* **8**, e75217 (2013).
20. Menssen, R. et al. Exploring the topology of the Gid complex, the E3 ubiquitin ligase involved in catabolite-induced degradation of gluconeogenic enzymes. *J. Biol. Chem.* **287**, 25602–25614 (2012).
21. Sherpa, D. et al. GID E3 ligase supramolecular chelate assembly configures multipronged ubiquitin targeting of an oligomeric metabolic enzyme. *Mol. Cell* **81**, 2445–2459 e2413 (2021).
22. Maitland, M. E. R., Lajoie, G. A., Shaw, G. S. & Schild-Poulter, C. Structural and functional insights into GID/CTLH E3 ligase complexes. *Int. J. Mol. Sci.* **23**, https://doi.org/10.3390/ijms23115863 (2022).
23. Ho, Y. et al. Systematic identification of protein complexes in *Saccharomyces cerevisiae* by mass spectrometry. *Nature* **415**, 180–183 (2002).
24. Lampert, F. et al. The multi-subunit GID/CTLH E3 ubiquitin ligase promotes cell proliferation and targets the transcription factor Hbp1 for degradation. *Elife* **7**, https://doi.org/10.7554/elife.35528 (2018).
25. Gottemukkala, K. V. et al. Non-canonical substrate recognition by the human WDR26-CTLH E3 ligase regulates prodrug metabolism. *Mol. Cell* **84**, 1948–1963 (2024).
26. Roxstrom-Lindquist, K. & Faye, I. The Drosophila gene Yippee reveals a novel family of putative zinc binding proteins highly conserved among eukaryotes. *Insect Mol. Biol.* **10**, 77–86 (2001).
27. Boltryk, S. D. et al. CRISPR/Cas9-engineered inducible gametocyte producer lines as a valuable tool for *Plasmodium falciparum* malaria transmission research. *Nat. Commun.* **12**, 4806 (2021).
28. Lasonder, E. et al. Integrated transcriptomic and proteomic analyses of *P. falciparum* gametocytes: molecular insight into sex-specific processes and translational repression. *Nucleic Acids Res.* **44**, 6087–6101 (2016).
29. Alano, P. et al. COS cell expression cloning of Pfg377, a *Plasmodium falciparum* gametocyte antigen associated with osmiophilic bodies. *Mol. Biochem. Parasitol.* **74**, 143–156 (1995).
30. de Koning-Ward, T. F. et al. The role of osmiophilic bodies and Pfg377 expression in female gametocyte emergence and mosquito infectivity in the human malaria parasite *Plasmodium falciparum*. *Mol. Microbiol.* **67**, 278–290 (2008).
31. Baum, J. et al. A conserved molecular motor drives cell invasion and gliding motility across malaria life cycle stages and other apicomplexan parasites. *J. Biol. Chem.* **281**, 5197–5208 (2006).
32. He, L. et al. *Plasmodium falciparum* GAP40 Plays an Essential Role in Merozoite Invasion and Gametocytogenesis. *Microbiol Spectr.* **11**, e0143423 (2023).
33. Maitland, M. E. R. et al. The mammalian CTLH complex is an E3 ubiquitin ligase that targets its subunit muskelin for degradation. *Sci. Rep.* **9**, 9864 (2019).
34. Gomes, A. R. et al. A transcriptional switch controls sex determination in *Plasmodium falciparum*. *Nature* **612**, 528–533 (2022).

35. Cao, W. X. et al. Precise Temporal Regulation of Post-transcriptional Repressors is required for an orderly Drosophila maternal-to-zygotic transition. *Cell Rep.* **31**, 107783 (2020).
36. Vidya, E. et al. EDC-3 and EDC-4 regulate embryonic mRNA clearance and biomolecular condensate specialization. *Cell Rep.* **43**, 114781 (2024).
37. de Bie, P. & Ciechanover, A. Ubiquitination of E3 ligases: self-regulation of the ubiquitin system via proteolytic and non-proteolytic mechanisms. *Cell Death Differ.* **18**, 1393–1402 (2011).
38. DeOliveira, C. C. & Crane, B. R. A structural decryption of cryptochromes. *Front. Chem.* **12**, 1436322 (2024).
39. Kleiner, O., Kircher, S., Harter, K. & Batschauer, A. Nuclear localization of the Arabidopsis blue light receptor cryptochrome 2. *Plant J.* **19**, 289–296 (1999).
40. Sakakida, Y. et al. Importin alpha/beta mediates nuclear transport of a mammalian circadian clock component, mCRY2, together with mPER2, through a bipartite nuclear localization signal. *J. Biol. Chem.* **280**, 13272–13278 (2005).
41. Chaves, I. et al. Functional evolution of the photolyase/cryptochrome protein family: importance of the C terminus of mammalian CRY1 for circadian core oscillator performance. *Mol. Cell Biol.* **26**, 1743–1753 (2006).
42. Qu, G. P., Jiang, B. & Lin, C. The dual-action mechanism of *Arabidopsis* cryptochromes. *J. Integr. Plant Biol.* **66**, 883–896 (2024).
43. Mohammed, M. et al. Single-cell transcriptomics reveal transcriptional programs underlying male and female cell fate during *Plasmodium falciparum* gametocytogenesis. *Nat. Commun.* **15**, 7177 (2024).
44. Luo, Y., Na, Z. & Slavoff, S. A. P-Bodies: Composition, Properties, and Functions. *Biochemistry* **57**, 2424–2431 (2018).
45. Sgromo, A. et al. Drosophila Bag-of-marbles directly interacts with the CAF40 subunit of the CCR4-NOT complex to elicit repression of mRNA targets. *RNA* **24**, 381–395 (2018).
46. Bawankar, P., Loh, B., Wohlbold, L., Schmidt, S. & Izaurralde, E. NOT10 and C2orf29/NOT11 form a conserved module of the CCR4-NOT complex that docks onto the NOT1 N-terminal domain. *RNA Biol.* **10**, 228–244 (2013).
47. Beelman, C. A. et al. An essential component of the decapping enzyme required for normal rates of mRNA turnover. *Nature* **382**, 642–646 (1996).
48. Hubstenberger, A. et al. P-Body purification reveals the condensation of repressed mRNA regulons. *Mol. Cell* **68**, 144–157 (2017).
49. Bruce, M. C., Carter, R. N., Nakamura, K., Aikawa, M. & Carter, R. Cellular location and temporal expression of the *Plasmodium falciparum* sexual stage antigen Pfs16. *Mol. Biochem. Parasitol.* **65**, 11–22 (1994).
50. Min, H. et al. The DEAD-box RNA helicase PfDOZI imposes opposing actions on RNA metabolism in *Plasmodium falciparum*. *Nat. Commun.* **15**, 3747 (2024).
51. Licon, M. H. et al. A positive feedback loop controls *Toxoplasma* chronic differentiation. *Nat. Microbiol.* **8**, 889–904 (2023).
52. Guerreiro, A. et al. Genome-wide RIP-Chip analysis of translational repressor-bound mRNAs in the *Plasmodium* gametocyte. *Genome Biol.* **15**, 493 (2014).
53. Decker, C. J. & Parker, R. P-bodies and stress granules: possible roles in the control of translation and mRNA degradation. *Cold Spring Harb. Perspect. Biol.* **4**, a012286 (2012).
54. Watzlowik, M. T. et al. *Plasmodium* blood stage development requires the chromatin remodeller Snf2L. *Nature* **639**, 1069–1075 (2025).
55. Zheng, H. & Xie, W. The role of 3D genome organization in development and cell differentiation. *Nat. Rev. Mol. Cell Biol.* **20**, 535–550 (2019).
56. Clapier, C. R., Iwasa, J., Cairns, B. R. & Peterson, C. L. Mechanisms of action and regulation of ATP-dependent chromatin-remodelling complexes. *Nat. Rev. Mol. Cell Biol.* **18**, 407–422 (2017).
57. Bunnik, E. M. et al. Changes in genome organization of parasite-specific gene families during the *Plasmodium* transmission stages. *Nat. Commun.* **9**, 1910 (2018).
58. Sancar, A. Regulation of the mammalian circadian clock by cryptochrome. *J. Biol. Chem.* **279**, 34079–34082 (2004).
59. Ozturk, N., VanVickle-Chavez, S. J., Akileswaran, L., Van Gelder, R. N. & Sancar, A. Ramshackle (Brwd3) promotes light-induced ubiquitylation of Drosophila Cryptochrome by DDB1-CUL4-ROC1 E3 ligase complex. *Proc. Natl. Acad. Sci. USA* **110**, 4980–4985 (2013).
60. Lobo, C.-A., Fujioka, H., Aikawa, M. & Kumar, N. Disruption of the Pfg27 locus by homologous recombination leads to loss of the sexual phenotype in *P. falciparum*. *Mol. Cell* **3**, 795–798 (1999).
61. Feng, Z., Chen, X., Wu, X. & Zhang, M. Formation of biological condensates via phase separation: characteristics, analytical methods, and physiological implications. *J. Biol. Chem.* **294**, 14823–14835 (2019).
62. Babu, M. M., van der Lee, R., de Groot, N. S. & Gsponer, J. Intrinsically disordered proteins: regulation and disease. *Curr. Opin. Struct. Biol.* **21**, 432–440 (2011).
63. van der Lee, R. et al. Classification of intrinsically disordered regions and proteins. *Chem. Rev.* **114**, 6589–6631 (2014).
64. Banani, S. F., Lee, H. O., Hyman, A. A. & Rosen, M. K. Biomolecular condensates: organizers of cellular biochemistry. *Nat. Rev. Mol. Cell Biol.* **18**, 285–298 (2017).
65. Gsponer, J., Futschik, M. E., Teichmann, S. A. & Babu, M. M. Tight regulation of unstructured proteins: from transcript synthesis to protein degradation. *Science* **322**, 1365–1368 (2008).
66. Dogga, S. K. et al. A single cell atlas of sexual development in *Plasmodium falciparum*. *Science* **384**, eadj4088 (2024).
67. Reid, A. J. et al. Single-cell RNA-seq reveals hidden transcriptional variation in malaria parasites. *Elife* **7**, https://doi.org/10.7554/elife.33105 (2018).
68. Real, E. et al. A single-cell atlas of *Plasmodium falciparum* transmission through the mosquito. *Nat. Commun.* **12**, 3196 (2021).
69. Hartwell, L. H. & Weinert, T. A. Checkpoints: controls that ensure the order of cell cycle events. *Science* **246**, 629–634 (1989).
70. Volz, J. C. et al. Essential Role of the PfRh5/PfRipr/CyRPA Complex during *Plasmodium falciparum* Invasion of Erythrocytes. *Cell Host Microbe* **20**, 60–71 (2016).
71. Ashdown, G. W. et al. A machine learning approach to define antimalarial drug action from heterogeneous cell-based screens. *Sci. Adv.* **6**, https://doi.org/10.1126/sciadv.aba9338 (2020).
72. Labun, K. et al. CHOPCHOP v3: expanding the CRISPR web toolbox beyond genome editing. *Nucleic Acids Res.* **47**, W171–W174 (2019).
73. Delves, M. J. et al. Routine in vitro culture of P. falciparum gametocytes to evaluate novel transmission-blocking interventions. *Nat. Protoc.* **11**, 1668–1680 (2016).
74. Baum, J., Maier, A. G., Good, R. T., Simpson, K. M. & Cowman, A. F. Invasion by *P. falciparum* merozoites suggests a hierarchy of molecular interactions. *Plos Pathog.* **1**, 299–309 (2005).
75. de Koning-Ward, T. F. et al. A newly discovered protein export machine in malaria parasites. *Nature* **459**, 945–U966 (2009).
76. Schindelin, J. et al. Fiji: an open-source platform for biological-image analysis. *Nat. Methods* **9**, 676–682 (2012).
77. Goedhart, J. SuperPlotsOfData-a web app for the transparent display and quantitative comparison of continuous data from different conditions. *Mol. Biol. Cell* **32**, 470–474 (2021).
78. Bianco, A. E. et al. A repetitive antigen of *Plasmodium falciparum* that is homologous to heat shock protein 70 of Drosophila melanogaster. *Proc. Natl. Acad. Sci. USA* **83**, 8713–8717 (1986).

79. Tian, L. et al. scPipe: A flexible R/Bioconductor preprocessing pipeline for single-cell RNA-sequencing data. *PLoS Comput. Biol.* **14**, e1006361 (2018).
80. Team RC. *R.: A Language and Environment for Statistical Computing*. (2025).
81. Chen, Y., Chen, L., Lun, A. T. L., Baldoni, P. L., Smyth, G. K. edgeR v4: powerful differential analysis of sequencing data with expanded functionality and improved support for small counts and larger datasets. *Nucleic Acids Res.* **53**, https://doi.org/10.1093/nar/gkaf018 (2025).
82. Chen, Y., Lun, A. T. & Smyth, G. K. From reads to genes to pathways: differential expression analysis of RNA-Seq experiments using Rsubread and the edgeR quasi-likelihood pipeline. *F1000Res.* **5**, 1438 (2016).
83. Robinson, M. D. & Oshlack, A. A scaling normalization method for differential expression analysis of RNA-seq data. *Genome Biol.* **11**, R25 (2010).
84. Law, C. W., Chen, Y., Shi, W. & Smyth, G. K. voom: Precision weights unlock linear model analysis tools for RNA-seq read counts. *Genome Biol.* **15**, R29 (2014).
85. Lun, A. T. L. & Smyth, G. K. No counts, no variance: allowing for loss of degrees of freedom when assessing biological variability from RNA-seq data. *Stat. Appl. Genet. Mol. Biol.* **16**, 83–93 (2017).
86. Smyth, G. K., Michaud, J. & Scott, H. S. Use of within-array replicate spots for assessing differential expression in microarray experiments. *Bioinformatics* **21**, 2067–2075 (2005).
87. Benjamini, Y., Drai, D., Elmer, G., Kafkafi, N. & Golani, I. Controlling the false discovery rate in behavior genetics research. *Behav. Brain Res.* **125**, 279–284 (2001).
88. Kariyawasam, H., Su, S., Voogd, O., Ritchie, M. E. & Law, C. W. Dashboard-style interactive plots for RNA-seq analysis are R Markdown ready with Glimma 2.0. *NAR Genom. Bioinform.* **3**, lqab116 (2021).
89. Bolger, A. M., Lohse, M. & Usadel, B. Trimmomatic: a flexible trimmer for Illumina sequence data. *Bioinformatics* **30**, 2114–2120 (2014).
90. Liao, Y., Smyth, G. K. & Shi, W. The R package Rsubread is easier, faster, cheaper and better for alignment and quantification of RNA sequencing reads. *Nucleic Acids Res.* **47**, e47 (2019).
91. Liao, Y., Smyth, G. K. & Shi, W. featureCounts: an efficient general purpose program for assigning sequence reads to genomic features. *Bioinformatics* **30**, 923–930 (2014).
92. Wisniewski, J. R., Zougman, A., Nagaraj, N. & Mann, M. Universal sample preparation method for proteome analysis. *Nat. Methods* **6**, 359–362 (2009).
93. Hughes, C. S. et al. Single-pot, solid-phase-enhanced sample preparation for proteomics experiments. *Nat. Protoc.* **14**, 68–85 (2019).
94. Wisniewski, J. R., Zougman, A. & Mann, M. Combination of FASP and StageTip-based fractionation allows in-depth analysis of the hippocampal membrane proteome. *J. Proteome Res.* **8**, 5674–5678 (2009).
95. Demichev, V. et al. dia-PASEF data analysis using FragPipe and DIA-NN for deep proteomics of low sample amounts. *Nat. Commun.* **13**, 3944 (2022).
96. Bruderer, R. et al. Extending the limits of quantitative proteome profiling with data-independent acquisition and application to acetaminophen-treated three-dimensional liver microtissues. *Mol. Cell Proteom.* **14**, 1400–1410 (2015).

Acknowledgements

The authors thank the Australian Red Cross Blood Service for blood and Till Voss (Swiss TPH) for providing the parasite line iGP2. This work was funded through grants from the National Health and Medical Research Council of Australia (NHMRC) (APP1194535, APP1176955, APP1177431) and supported by the Victorian State Government Operational Infrastructure Support grant (Institutional grant) and Australian Government NHMRC IRIISS.

Author contributions

D.S.M., A.F.C. and M.W.A.D. conceptualised the studies, wrote the draft, and all authors contributed to data analysis as well as reviewing, editing and approving the manuscript. D.S.M., S.L., S.K., N.J. and M.W.A.D. constructed transgenic parasites and performed phenotypic analysis. D.S.M., S.L., B.B. and A.J. performed and analysed the analysis of RNA from GD1 immunoprecipitations. S.A.C., D.K. and D.S.M. performed and analysed the ubiquitin proteomics data. D.S.M., N.D.G. and K.R. performed and analysed microscopy of transgenic parasites. S.W.S. produced recombinant Pfg377 protein for antibody generation. PH analysed the transcriptome data. D.S.M., V.V., S.S., J.Y. and L.F.D. performed and analysed the proteomics. K.R., A.C., C.D.G. and G.I.M. performed and analysed the mosquito transmission data. J.S.M. contributed significant support and concepts for the manuscript. C.J.T. suggested the investigation of the PfGID complex in *P. falciparum* and contributed to the conceptualisation of the study.

Competing interests

The authors have no competing interests with the studies described.

Additional information

Supplementary information The online version contains supplementary material available at https://doi.org/10.1038/s41467-026-69183-9.

Correspondence and requests for materials should be addressed to Danushka S. Marapana, Matthew W. A. Dixon or Alan F. Cowman.

Peer review information *Nature Communications* thanks Elizabeth Winzeler, who co-reviewed with Fu-Hsuan Ko and the anonymous reviewers for their contribution to the peer review of this work. A peer review file is available.